PERGAMON

Applied Geochemistry 16 (2001) 1567–1593

Applied Geochemistry

www.elsevier.com/locate/apgeochem

Geochemical and mineralogical controls on trace element release from the Penn Mine base-metal slag dump, California

Michael B. Parsons [a,*], Dennis K. Bird [a], Marco T. Einaudi [a], Charles N. Alpers [b]

[a] *Department of Geological and Environmental Sciences, Stanford University, Stanford, CA 94305-2115, USA*
[b] *US Geological Survey, 6000 J Street, Sacramento, CA 95819-6129, USA*

Received 25 October 1999; accepted 30 December 2000

Editorial handling by D. Runnells

Abstract

Base-metal slag deposits at the Penn Mine in Calaveras County, California, are a source of environmental contamination through leaching of potentially toxic elements. Historical Cu smelting at Penn Mine (1865–1919) generated approximately 200,000 m^3 of slag. The slag deposits, which are flooded annually by a reservoir used for drinking water and irrigation, also may be in contact with acidic ground waters (pH < 4) from the adjacent mine area. Slags vary from grey to black, are glassy to crystalline, and range in size from coarse sand to large (0.6×0.7×1.5 m), tub-shaped casts. Metals are hosted by a variety of minerals and two glass phases. On the basis of mineralogy, slags are characterized by 4 main types: *fayalite-rich, glassy, willemite-rich*, and *sulfide-rich*. The ranges in metal and metalloid concentrations of 17 slag samples are: As, 0.0004–0.92; Ba, 0.13–2.9; Cd, 0.0014–1.4; Cu, 0.18–6.4; Pb, 0.02–11; and Zn, 3.2–28 wt.%. Leachates from Toxicity Characteristic Leaching Procedure tests (acetic acid buffered at pH 4.93) on two willemite-rich slags contained Cd and Pb concentrations (up to 2.5 and 30 mg/l, respectively) in excess of US Environmental Protection Agency (USEPA) regulatory limits. Analyses of filtered (0.45 μm) water, collected within the flooded slag dump during reservoir drawdown, reveal concentrations of Cd (1.7 μg/l), Cu (35 μg/l), and Zn (250 μg/l) that exceed USEPA chronic toxicity guidelines for the protection of aquatic life. Data from field and laboratory studies were used to develop geochemical models with the program EQ3/6 that simulate irreversible mass-transfer between slag deposits and reservoir waters. These models include kinetic rate laws for abiotic sulfide oxidation and surface-controlled dissolution of silicates, oxides, and glass. Calculations demonstrate that the main processes controlling dissolved metal concentrations are (1) dissolution of fayalite, willemite, and glass; (2) sulfide oxidation; and (3) secondary phase precipitation. Close agreement between model results and measured concentrations of Al, Ba, Cu, Fe, SiO_2, and SO_4 in the slag dump pore waters suggests that the dissolved concentrations of these elements are controlled by solubility equilibrium with secondary phases. Differences between predicted and measured Cd and Pb concentrations imply that field weathering rates of glass and sulfides are approximately two orders of magnitude lower than laboratory rates. Overprediction of Pb release may also reflect other attenuation processes in the natural system, such as sorption or coprecipitation.

1. Introduction

The extraction of metals from sulfide ores results in the production of a variety of hazardous wastes through mining, milling, and smelting activities (Moore and Luoma, 1990). Unlike slags resulting from iron and steel production (ferrous slags), those from base-metal

* Corresponding author at Geological Survey of Canada (Atlantic), Bedford Institute of Oceanography, 1 Challenger Drive, PO Box 1006, Dartmouth, Nova Scotia, Canada B2Y 4A2. Tel.: +1-902-426-7363; Fax: +1-902-426-4104.

E-mail address: parsons@agc.bio.ns.ca (M.B. Parsons).

0883-2927/01/$ - see front matter
PII: S0883-2927(01)00032-4

smelters typically contain elevated levels of potentially toxic elements (e.g. As, Ba, Cd, Cu, Pb, Zn), and are a possible source of surface and ground water contamination (e.g. Tack et al., 1993; Kucha et al., 1996; Gee et al., 1997; Manz and Castro, 1998). However, smelter slags have traditionally been considered relatively inert in most weathering environments because many of the toxic elements are contained in low solubility silicates, oxides, and glass. Both ferrous and base-metal slags are commonly used as construction materials (e.g. sandblasting grit, road ballast, cement additives, roofing shingles), and large slag dumps exist near many smelting operations (Emery, 1978; Queneau et al., 1991; Flett and Riddler, 1992; Wilson, 1994; Mandin et al., 1997; Bayless et al., 1998; Proctor et al., 2000).

Most previous studies of slag leaching have been restricted to laboratory-based batch extraction tests, which involve agitation of a specific quantity of crushed slag in a predefined volume of extraction fluid (leachant), without leachant renewal (e.g. Johnson et al., 1982; Robbins et al., 1983; Woodley and Walters, 1986; May and Peterson, 1991; Gül, 1994; Jahanshahi et al., 1994; Lagos and Luraschi, 1997; Male et al., 1997; Manz and Castro, 1998; Proctor et al., 2000). In North America, all of the regulatory leach protocols used for solid waste classification (e.g. as hazardous or non-hazardous) are batch extraction tests. Some studies have employed dynamic leach tests, which involve intermittent or continuous leachant renewal (e.g. Tack et al., 1993; Fällman and Hartlén, 1994; Kontopoulos et al., 1996; Koren et al., 1996; Bäverman et al., 1997). To predict the long-term (i.e. tens to hundreds of years) leaching behavior of slags, some researchers have combined the results of dynamic leach tests with geochemical computer models (e.g. Tack et al., 1993; Bäverman et al., 1997; Mandin et al., 1997). The predictive capability and reliability of these models has been limited by incomplete characterization of slag mineralogy and reactive surface area, unrealistic equilibrium assumptions, and a lack of field data with which to compare model results. Although some progress has been made in developing a leach test protocol for slags, many questions remain concerning the mechanisms and rates of slag leaching reactions, and the relationship between leachate compositions from laboratory-based tests and measured water compositions in the field (Wilson, 1994; van der Sloot et al., 1997).

The Penn Mine slag dump in California, submerged annually by a reservoir used for drinking water and irrigation (Camanche Reservoir), provides an excellent natural laboratory to study the release of trace elements from base-metal slags over a wide range of geochemical conditions. Detailed characterization of slag mineralogy and field observations of naturally weathered slags are used to identify the main sources of potentially toxic elements. Measurements of water compositions in the field and in laboratory extraction tests provide information on the rates and extent of slag leaching reactions. Results of field and laboratory investigations are used to constrain geochemical models that simulate the natural weathering reactions of base-metal slag deposits, and the potential impact of these processes on surface and ground waters.

2. Description of study area

2.1. Geology of Penn Mine

The Penn Mine is an abandoned Cu–Zn mine located in the western Sierra Nevada foothills, in Calaveras County, California (Fig. 1). The mine forms part of the Foothill Cu–Zn belt, a NW-trending group of volcanogenic massive sulfide deposits that extends for 400 km along the western flank of the Sierra Nevada (Martin, 1988). Bedrock at Penn Mine consists of a Jurassic metavolcanic unit (Gopher Ridge volcanics) that hosts most of the sulfide deposits, a Jurassic metasedimentary unit (Salt Spring slate), and an auriferous Tertiary conglomerate that uncomformably overlies the other units (Peterson, 1985).

Ore consists of massive, stratiform sulfide lenses that dip steeply eastward parallel to bedding and regional schistosity, which strikes approximately N 30° W. The lenticular bodies of massive ore ranged in size from 50 to 300 m along pitch, 30–135 m in width, and 1.3–10 m in thickness. Processed ores consisted mainly of pyrite (FeS_2), chalcopyrite ($CuFeS_2$), and sphalerite [(Zn,Fe,Cd)S] with minor bornite (Cu_5FeS_4), chalcocite (Cu_2S), covellite (CuS), galena (PbS), and tetrahedrite-tennantite [$(Cu,Fe,Ag,Zn)_{12}(Sb,As)_4S_{13}$]. Gangue minerals include barite ($BaSO_4$), quartz (SiO_2), calcite ($CaCO_3$), and gypsum ($CaSO_4{\cdot}2H_2O$) (Heyl et al., 1948; Schmidt, 1978; Peterson, 1988).

2.2. Wastes produced by mining, milling, and metallurgical operations

The Penn Mine was one of the largest producers of Cu in the Foothill Cu–Zn belt from the early 1860s to the late 1950s. In 1952, total production was estimated at 883,401 metric tons of ore containing 37,437 metric tons Cu, 10,068 metric tons Zn, 559 metric tons Pb, 60,691 kg Ag, and 1,921 kg Au (Clark and Lydon, 1962). Wastes from mining, milling, and smelting include waste rock dumps, mill tailings, one metallurgical coke pile, and one smelter slag dump.

Three separate smelters operated at Penn Mine between 1865 and 1919. The first smelter, in operation from 1865 to 1867, produced a 35 wt.% Cu matte from ores averaging 6–10 wt.% Cu. Slags and other wastes from these early smelting operations were dumped directly into the adjacent Mokelumne River (Browne, 1868). A second smelter, which operated from 1889 to

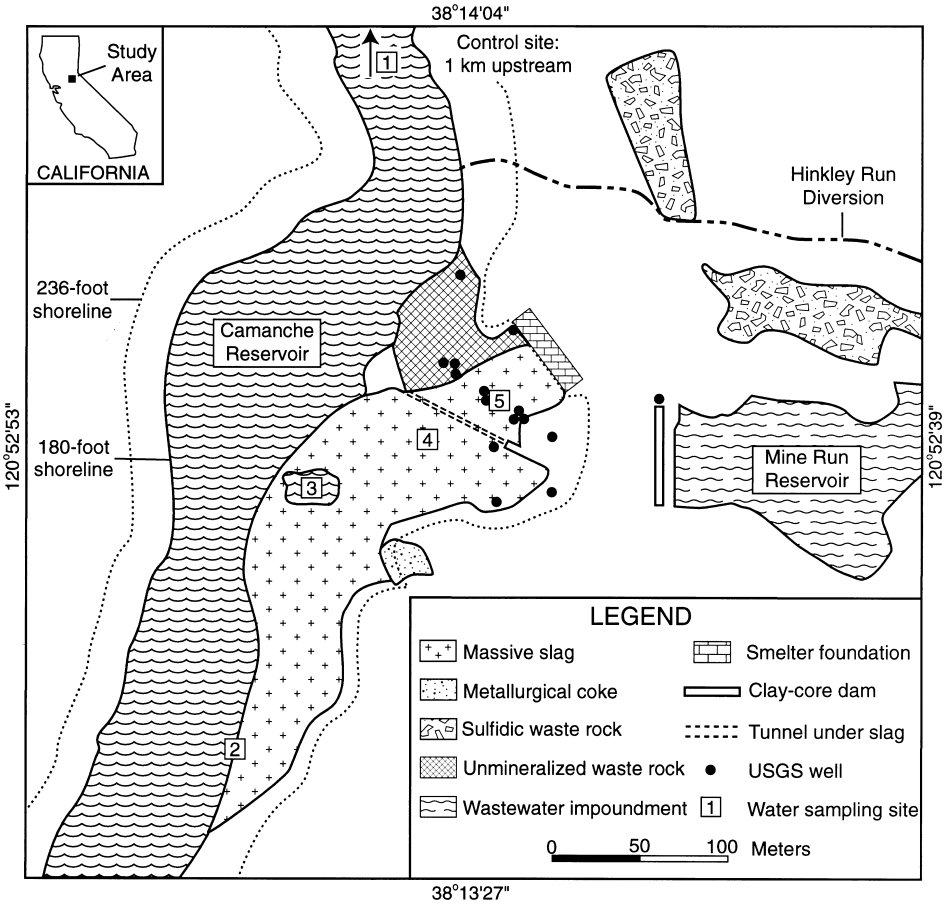

Fig. 1. Western edge of Penn Mine site showing slag dump and waste rock piles adjacent to Camanche Reservoir. Boxed numbers indicate the location of water sampling sites: (1) upstream control, (2) downstream edge of slag dump, (3) depression in slag dump, (4) US Bureau of Mines — test pit No. 1, and (5) US Geological Survey monitoring well GS-9 (modified from Wiebelt and Ricker, 1948; Davy Environmental, 1993; Hamlin and Alpers, 1996).

1890, produced a 40 wt.% Cu matte from ores averaging 8 wt.% Cu (Lang, 1907). The third period of Cu smelting began with the construction of a new smelter in 1899 that produced a final product of 50–60 wt.% Cu matte from ore averaging 4.6 wt.% Cu and, after 1902, 4.8 wt.% Cu (Aubury, 1908). Between 1899 and 1919, approximately 725,747 metric tons of Cu–Zn ore were smelted; the resulting molten slag was tapped into large slag pots and dumped on top of the earlier slag piles in a 450-m-long area immediately adjacent to the Mokelumne river channel (Fig. 1). The last smelter was shut down in 1919 (Julihn and Horton, 1938).

In 1942, the US Bureau of Mines (USBM) investigated the feasibility of extracting Zn and Cu from the Penn Mine slag deposits. Approximately 150 samples of slag were collected from shafts and trenches excavated in the dump, and assay results indicated average Zn and Cu contents of 6.5 and 0.37 wt.%, respectively. Metallurgical tests on a composite sample (with 5.6 wt.% Zn) volatilized 22–29 wt.% of the total Zn content, but these recoveries were considered too low for profitable extraction (Wiebelt and Ricker, 1948).

Completion of the Camanche dam in 1963 flooded the Mokelumne river from 15 km downstream of Penn Mine to approximately 1.5 km upstream. The spillway elevation of the dam is 72 m above sea level (ASL); the slag dump at Penn Mine is partly flooded when the level of the reservoir pool is greater than about 53 m ASL, and fully submerged when the reservoir level reaches 67 m ASL (Finlayson and Rectenwald, 1978). The present study focuses on interactions between the slag dump and the Camanche Reservoir.

2.3. History of pollution at Penn Mine

Acid, metal-rich surface runoff from Penn Mine has caused contamination and fish kills in the Mokelumne river basin since mining first began in the 1860s (Shaw and

Towers, 1937; Cordone, 1962; Finlayson and Rectenwald, 1978; Slotton and Reuter, 1995). These acidic waters result from oxidation of sulfide minerals in both surface and subsurface environments (Davy Environmental, 1993). The US Geological Survey (USGS) (Hamlin and Alpers, 1995, 1996; Alpers et al., 1999) has documented acidic ground waters with elevated concentrations of metals and SO_4 flowing through a fractured metavolcanic aquifer from the Mine Run reservoir towards the Camanche Reservoir (Fig. 1). This ground water flows below the slag dump, and may be in contact with the base of the dump during periods of high ground-water discharge. In 1997, federal and state regulatory agencies approved a remediation plan for long-term pollution control at Penn Mine (Golder Associates, 1997). Construction of a lined landfill for sulfidic mine wastes began in June 1998 [East Bay Municipal Utility District (EBMUD), written comm., 1998]. The slag dump is outside the boundaries of the remediation project, and is not slated for clean-up.

3. Methodology

3.1. Sampling and analysis of smelter slags

Samples of smelter slag collected for this study consist of two distinct groups. Thirty-three samples were collected from the surface and interior of the slag pot casts, as well as from glassy slag that was poured as a molten liquid over these casts. A second group of 8 samples are drill cuttings collected in 1991 and 1992 during construction by the USGS of ground-water monitoring wells through the slag dump (Hamlin and Alpers, 1995, 1996). Estimates of the relative abundance of each type of slag were recorded during field mapping.

Following examination using a binocular microscope, polished thin sections were prepared for 20 representative slag samples. Electron microprobe analyses were performed at Stanford University on a JEOL JXA-733A Superprobe with 5 wavelength-dispersive spectrometers and a Be-window SiLi energy dispersive (EDS) detector. Each spectrum was acquired for 20 s using an accelerating voltage of 15–20 keV, a beam current of 15 nA, and a spot size of 1–10 μm. The CITZAF matrix correction program was used to account for the effects of atomic number, X-ray absorption, and secondary fluorescence on measured X-ray intensities. Standard reference materials were used to calibrate the instrument for quantitative analysis of silicates, oxides, sulfides, and glass. Instrument precision for 10 analyses of a willemite standard was approximately 0.5%. Relative accuracy for major elements is between 1.5 and 2.0%. Transmitted and reflected light microscopy, X-ray powder diffraction (XRD), and scanning electron microscopy (SEM) were also used to identify primary phases and associated secondary (weathering-related) minerals.

Chemical compositions of 17 samples (average mass: 400 g) of slag were determined using inductively coupled plasma–atomic emission spectrometry (ICP–AES) following $HF/HNO_3/HClO_4$ digestion. Some samples had concentrations of Ba, Cd, Cu, Pb, and Zn greater than the upper concentration limits for ICP-AES (0.5 wt.% Cd; 1 wt.% Zn, Ba; 3 wt.% Cu, Pb); these elements were assayed using X-ray fluorescence spectroscopy (XRF) following $LiBO_2$ fusion. Total S in all samples was measured using a LECO S analyzer (ICP-AES, XRF, and LECO analyses performed by XRAL Laboratories, Ontario, Canada). Results for blind duplicates and standard reference materials indicate precision and accuracy are about 5% for major and minor oxides, and 5–10% for trace elements.

3.2. Regulatory leaching tests

Two samples of slag were submitted to American Assay Laboratories (Sparks, Nevada) for characterization using the Toxicity Characteristic Leaching Procedure (TCLP) and the Synthetic Precipitation Leaching Procedure (SPLP), as outlined by the US Environmental Protection Agency (USEPA, 1994, 1996). The TCLP is a regulatory leach protocol that involves crushing a sample to pass a 9.5-mm sieve, followed by end-over-end agitation of 100 g of sample for 18 ± 2 h in buffered acetic acid (pH 2.88 or 4.93, depending on buffering capacity of waste) at a 20:1 liquid-to-solid ratio (USEPA, 1996). The SPLP is very similar to the TCLP, but uses simulated acid rain (a mixture of 60/40 wt.% H_2SO_4/HNO_3; pH 4.20 or 5.00 depending on site location) as the leachant (USEPA, 1994). Concentrations of As, Ba, Cd, Cr, Cu, Pb, Sb, and Zn in the filtered (0.6–0.8-μm) TCLP and SPLP leachates were determined using ICP–AES. Mercury was analyzed using cold-vapor–atomic absorption spectroscopy (CV–AAS).

3.3. Water-quality sampling and analysis

Lake water was sampled at 4 sites in the Camanche Reservoir using an acrylic Van Dorn-style water sampler. Two or 3 samples were collected at each station — 1 from just below the surface, and 1 or 2 at measured intervals in the water column. In situ field measurements of temperature, pH, Eh, specific conductance, and dissolved O_2 (DO) were taken at each sampling site using a multiparameter water-quality monitoring instrument. To determine background metal concentrations in the reservoir inflow, water was sampled from a control site approximately 1 km upstream of Penn Mine (site 1, Fig. 1). The remaining 3 sites were located adjacent to, or directly over, the flooded slag dump (sites 2–4, Fig. 1). This sampling program was designed to evaluate seasonal changes in water quality, and included sampling of lake water in August 1996 (during prolonged flooding of the dump), March 1997 (immediately following reservoir drawdown),

January 1998 (during a rise in reservoir level), and March 1998 (during rapid reservoir drawdown) (Fig. 2). In March 1997, a water sample was also collected from USGS well GS-9 (site 5, Fig. 1) to assess ground-water quality near the base of the slag dump. This well penetrates slag to a depth of 3.3 m, bottoms in metavolcanic rock at 6.1 m, and is lined by perforated, 6-inch (15.3 cm)-diameter polyvinyl chloride casing along the entire depth of the well (Hamlin and Alpers, 1996). Prior to sampling, the well was purged using a polyethylene bailer until the pH, specific conductance, and temperature of the ground water had stabilized.

Collection and processing of all water samples was conducted using techniques and quality-control methods similar to those outlined by Horowitz et al. (1994) and Ficklin and Mosier (1999). Samples for cation, anion, and alkalinity analyses were filtered in the field through 47-mm diameter, 0.45-μm pore-size cellulose acetate membranes. To determine the effect of filter pore size on trace element concentrations in filtrates, unfiltered lake water was collected in March 1997, January 1998, and March 1998, and selected samples were also processed using 47-mm diameter, 0.10-μm pore-size cellulose acetate membranes. In March 1997, surface samples of lake water were obtained at sites 1 and 2 for tangential-flow ultrafiltration using a Millipore Minitan system with a 10,000 Dalton filter membrane, equivalent to a pore diameter of 0.005 μm (Millipore Corporation, 1993). Samples for trace element and major cation analysis were acidified in the field with Ultrex-grade HNO_3 to a pH < 2.0. All samples were chilled on ice, and samples for cation and anion analysis were couriered to analytical laboratories within 48 h of collection.

Total concentrations of 66 trace elements and major cations were determined using inductively coupled plasma–mass spectrometry (ICP–MS) at Activation Laboratories Ltd. in Wheat Ridge, Colorado. Three anions (Cl, F, and SO_4) were analyzed by ion chromatography at the USGS Water Quality Service Unit in Ocala, Florida. Alkalinity was measured by Gran titration using a Hach digital titrator with 0.16 N H_2SO_4. During each round of field sampling, reagent-grade water was processed through all equipment and sampling steps to evaluate potential contamination. Traces of several elements were generally present within the field blanks — the values for these constituents are considered a lower detection limit for all samples. Blind duplicates were also submitted with each batch of samples — based on these replicate analyses, the precision for all ICP–MS analyses reported in this paper is ±10%.

4. Results

4.1. Physical characteristics of the Penn Mine slag deposits

The Penn Mine slags are grey to black, glassy to crystalline, and commonly have an iridescent luster. Where

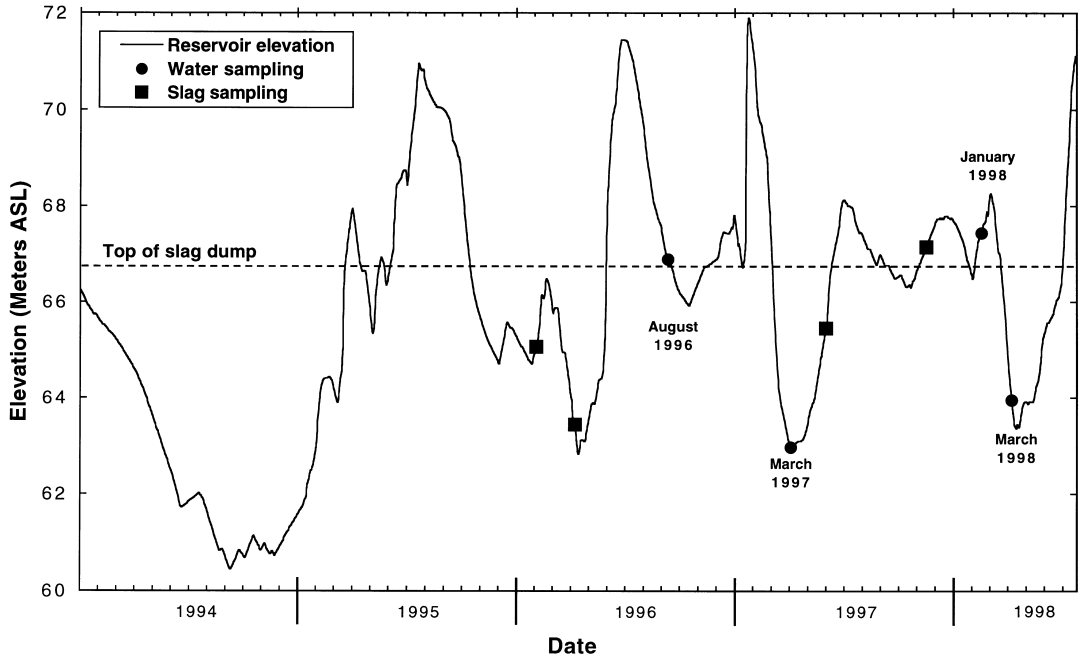

Fig. 2. Camanche Reservoir surface elevation from January 1994 to June 1998. The sampling program for this study evaluated seasonal changes in the weathering environment of the slag dump, and included sampling of slag (squares) and lake and ground water (circles) at various times throughout the year.

dumped in a molten state, slag is glassy and displays flow structures. Most individual fragments are angular, ranging in size from coarse sand to large (0.6×0.7×1.5 m) tub-shaped casts (Fig. 3). The top surfaces of these casts are vesiculated, and contain abundant quartz fragments and relict sulfide minerals. These sulfides readily oxidize, as indicated by the reddish-brown hydrous ferric oxides (HFO) that stain the top surfaces of the casts. Some slags exhibit thin, discontinuous coatings of other secondary minerals, but these are not common, possibly as a result of annual inundation by the Camanche Reservoir. XRD and SEM analyses have identified secondary barite ($BaSO_4$) (Fig. 4d), cerussite ($PbCO_3$), chalcanthite ($CuSO_4{\cdot}5H_2O$), hydrozincite ($Zn_5(CO_3)_2(OH)_6$), and malachite ($Cu_2CO_3(OH)_2$), in addition to HFO.

The heterogeneous nature of the Penn Mine slags, and the thin veneer of lake sediments that covers much of the dump, complicate an accurate estimate of the volume of smelter waste and the distribution of slag minerals. Using test pit data from Wiebelt and Ricker (1948), drill logs from Hamlin and Alpers (1996), and a large-scale base map of the slag dump area provided by EBMUD, the dump volume calculated by sectional method is approximately 200,000 m^3. The porosity of the slag deposits ranges from near 0% to greater than 30%.

4.2. Chemical composition of minerals and glasses in slag

Slags are composed of various silicate, oxide, sulfide, and glass phases (Tables 1–3). Silicates include Zn-rich fayalite, willemite, Ba-feldspar (hyalophane), quartz, and minor pyroxene. Oxide minerals are zincian spinels (gahnite, franklinite), magnetite, and minor Zn-rich hematite. Two main assemblages of sulfide minerals occur in the slags: (1) pyrite + chalcopyrite + sphalerite ± galena ± bornite ± covellite, and (2) pyrrhotite + cubanite + sphalerite/wurtzite ± Cu–Fe–S intermediate solid solutions (ISS). The first is restricted to the top surfaces of the slag pot casts, and represents relict sulfides that were not fused in the smelter. Sulfide minerals in the second assemblage are widely dispersed throughout the slags, commonly intergrown with fayalite crystals, and appear to have formed from sulfide melt during cooling of the slag. Many slags also contain a Pb–Zn–Cu–Cd–Ba-rich interstitial glass phase, and small blebs of metallic Pb and Cu.

4.2.1. Zinc-rich olivine $(Fe,Zn)_2SiO_4$

Zinc-rich fayalite is the most abundant phase. It occurs as grey, acicular, skeletal crystals up to 4 cm long, intergrown with sulfides (mainly cubanite, pyrrhotite, and wurtzite) within a Pb–Zn–Cu–Cd–Ba-rich glassy matrix (Fig. 4a). This mineral contains an average of 6.8 wt.% ZnO (Table 1), and co-exists with all phases except for willemite, gahnite, and franklinite.

4.2.2. Interstitial glass

The matrix in most slags (e.g. Fig. 4a and b) consists of amorphous material that has a highly variable composition. As shown in Fig. 4c, this phase has dissolved more rapidly than the fayalite crystals, resulting in leached cavities on the surfaces of naturally weathered

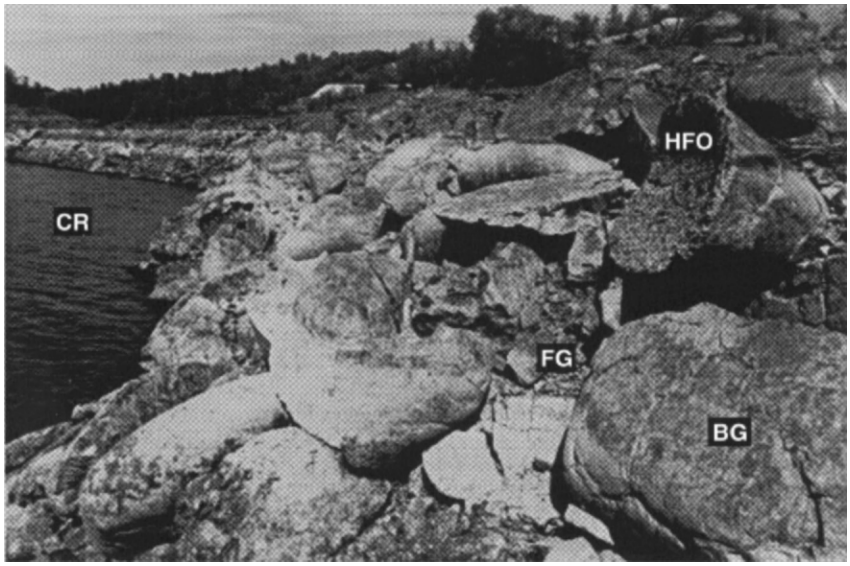

Fig. 3. Downstream edge of slag dump showing tub-shaped slag pot casts. The rounded surfaces of these casts consist mainly of bulk glass (BG), whereas the upper surfaces contain abundant relict sulfide minerals that oxidize to form hydrous ferric oxides (HFO). Finer-grained slag (FG) fills the voids between casts. During inundation by Camanche Reservoir (CR), water sampling site number 2 (Fig. 1) was located directly over this area.

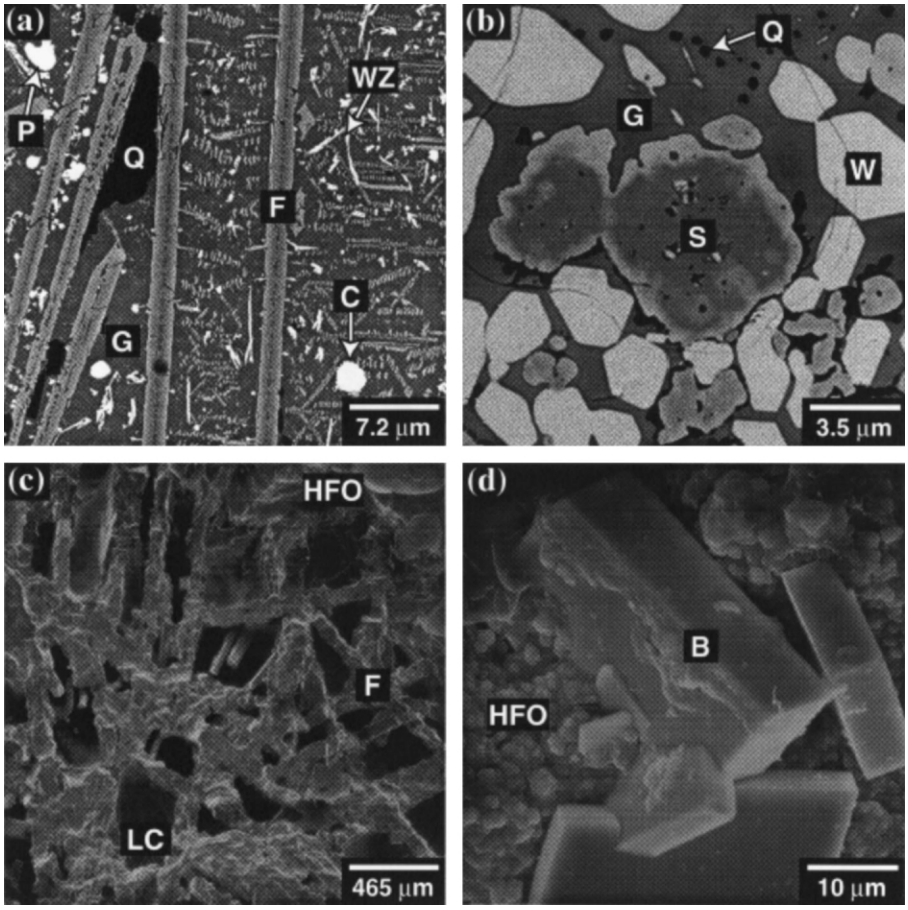

Fig. 4. Backscattered electron (BSE) and secondary electron (SE) images of unweathered and weathered slags: (a) BSE image of unweathered fayalite-rich slag showing acicular fayalite crystals (F), quartz (Q), cubanite (C), pyrrhotite (P), wurtzite (WZ), and interstitial glass (G); (b) BSE image of unweathered willemite-rich slag composed of spinel (S) (zoned from Al-rich core (gahnite) to Fe-rich rim (franklinite)), willemite (W), quartz (Q), and interstitial glass (G); (c) SE image of weathered fayalite-rich slag surface showing fayalite crystals (F), secondary hydrous ferric oxide (HFO), and leached cavities (LC) partially filled with HFO. Comparison with (a) reveals that interstitial glass and sulfides have reacted more quickly than fayalite, resulting in leached cavities between the fayalite crystals; (d) Secondary barite (B) intergrown with hydrous ferric oxide (HFO) precipitates on the surface of a weathered fayalite-rich slag. Note that the brightness of a phase in BSE images is proportional to its mean atomic number, Z (phases with a greater Z appear brighter), whereas contrast in SE images mainly reflects variations in surface topography.

slags. This observation has important environmental implications, because the interstitial glass averages 34 wt.% PbO, 5.0 wt.% ZnO, 2.7 wt.% CuO, 2.5 wt.% CdO, and 1.3 wt.% BaO (Table 1).

4.2.3. Bulk glass

Rapid quenching of molten slag produced a black, amorphous material containing traces of metal sulfides (matte prills), pyroxene, and metallic Pb and Cu. The rounded surfaces of many slag pot casts consist mostly of this glassy material (Fig. 3). The bulk glass contains an average of 1.7 wt.% BaO and 5.6 wt.% ZnO, and has a much higher FeO_T (total Fe) content (28 wt.%) than the interstitial glass (Table 1).

4.2.4. Willemite Zn_2SiO_4

Light-green, subhedral willemite crystals are the most common phase found in slags near the smelter foundation (Fig. 4b). Willemite crystals range in size from <1 μm to about 1 mm, and contain an average of 69 wt.% ZnO (Table 1). At Penn Mine, secondary hydrozincite forms thin surface coatings on the willemite-rich slags.

4.2.5. Zincian spinels

Bluish-green spinels with compositions intermediate between gahnite ($ZnAl_2O_4$) and franklinite ($ZnFe^{III}_2O_4$) occur throughout the willemite-rich slags. Most spinels are zoned, typically with Al-rich cores and Fe-rich rims (Fig. 4b). This phase forms grains up to 0.5 mm in size,

Table 1
Electron microprobe analyses of silicates, oxides, bulk glass, and interstitial glass in Penn Mine slag (wt.%)

Phase[a]	SiO_2	TiO_2	Al_2O_3	Cr_2O_3	FeO_T[b]	Fe_2O_3	MnO	MgO	BaO	CaO	CuO	ZnO	CdO	PbO	Na_2O	K_2O	Total	n[c]
Fayalite																		
Min (Zn)	43.94	0.10	3.28	< 0.02	41.16		0.04	1.65	0.06	3.02	< 0.03	5.51	< 0.04	0.18	< 0.03	< 0.02	98.93	
Max (Zn)	30.65	0.02	0.13	< 0.02	50.44		0.05	7.62	0.20	0.26	0.10	9.14	< 0.04	< 0.05	< 0.03	0.02	98.65	
Average	32.07	0.03	0.27	< 0.02	50.42		0.06	8.63	0.12	0.42	0.11	6.83	< 0.04	0.09	< 0.03	0.02	98.91	30
Interstitial glass																		
Min (Pb)	61.63	0.31	11.17	< 0.02	1.58		0.07	0.21	1.74	3.58	< 0.03	6.26	0.39	8.81	0.74	3.01	99.50	
Max (Pb)	25.67	0.03	2.92	< 0.02	0.84		< 0.02	0.37	< 0.04	3.17	2.50	2.24	3.36	58.94	< 0.03	< 0.02	100.05	
Average	41.39	0.13	6.69	< 0.02	1.61		< 0.02	0.57	1.30	2.77	2.72	5.00	2.46	33.55	0.37	1.23	99.77	8
Bulk glass																		
Min (Zn)	46.46	0.30	8.77	< 0.02	26.30		0.03	3.47	1.94	4.64	< 0.03	4.72	< 0.04	< 0.05	0.13	1.37	98.14	
Max (Zn)	44.92	0.31	8.79	< 0.02	30.24		0.01	2.32	2.11	2.54	< 0.03	6.43	< 0.04	0.07	0.12	1.42	99.30	
Average	45.50	0.32	8.61	< 0.02	28.51		0.04	3.20	1.75	3.49	0.05	5.58	< 0.04	0.06	0.14	1.38	98.63	15
Willemite																		
Min (Zn)	25.70	0.03	0.80	< 0.02	2.73		< 0.02	2.34	< 0.04	< 0.02	1.20	65.26	0.20	0.08	< 0.03	< 0.02	98.35	
Max (Zn)	27.46	0.02	0.42	< 0.02	1.13		0.03	1.31	< 0.04	< 0.02	< 0.03	70.40	0.04	< 0.05	0.29	< 0.02	101.10	
Average	27.53	0.02	0.34	< 0.02	0.76		< 0.02	2.32	< 0.04	< 0.02	0.49	68.63	0.11	0.07	0.14	< 0.02	100.20	26
Zincian spinel																		
Min (Zn)	1.96	1.96	11.45	0.09	25.75	46.48	< 0.02	1.03	0.36	0.19	0.14	9.79	< 0.04	< 0.05	< 0.03	0.12	99.35	
Max (Zn)	0.43	0.25	49.44	0.02	2.09	6.39	< 0.02	0.21	< 0.04	< 0.02	0.21	41.39	< 0.04	< 0.05	< 0.03	< 0.02	100.44	
Average	0.51	0.83	29.04	0.05	6.58	32.02	0.02	0.68	0.09	0.06	1.02	32.45	< 0.04	< 0.05	< 0.03	0.03	99.60	21
Magnetite																		
Min (Zn)	0.70	1.15	6.05	0.13	28.56	58.00	0.04	0.88	0.16	< 0.02	< 0.03	4.67	< 0.04	< 0.05	< 0.03	< 0.02	100.33	
Max (Zn)	0.12	0.76	11.26	< 0.02	15.68	54.10	< 0.02	3.46	0.15	< 0.02	< 0.03	13.61	< 0.04	< 0.05	< 0.03	< 0.02	99.15	
Average	0.99	1.49	8.26	0.14	25.98	57.42	0.04	1.42	0.34	0.16	< 0.03	8.60	< 0.04	< 0.05	< 0.03	0.07	99.03	13
Hyalophane																		
Min (Ba)	50.34	0.06	21.25	< 0.02	0.88		< 0.02	< 0.02	12.08	0.64	< 0.03	0.18	< 0.04	5.70	0.61	7.34	99.10	
Max (Ba)	50.13	0.07	21.50	< 0.02	0.79		< 0.02	0.02	14.63	0.65	< 0.03	0.38	< 0.04	4.90	0.64	6.98	100.70	
Average	48.73	0.05	20.55	< 0.02	0.79		< 0.02	0.02	13.14	0.42	< 0.03	0.21	< 0.04	5.21	0.88	6.52	100.31	10

[a] For each phase, full analyses are included for the maximum and minimum concentrations of the metal identified in parentheses.
[b] Total Fe calculated as FeO for all phases except zincian spinel and magnetite, for which the Fe^{2+}/Fe^{3+} ratio was estimated using stoichiometry assumptions in Droop (1987).
[c] n, Number of electron microprobe analyses.

and contains an average of 32 wt.% ZnO, and 1.0 wt.% CuO (Table 1).

4.2.6. Magnetite ($Fe^{II}Fe^{III}_2O_4$)

Magnetite forms small (< 5 μm) euhedral crystals that are disseminated throughout most of the fayalite-bearing slags. The magnetite contains an average of 8.6 wt.% ZnO and 0.34 wt.% BaO (Table 1).

4.2.7. Hyalophane ($K,Na,Ba)(Al,Si)_4O_8$

Hyalophane occurs as subhedral crystals (generally < 100 μm in size) interstitial to willemite and zincian spinel. This mineral commonly shows oscillatory zoning with varying amounts of Ba and K, and contains an average of 13 wt.% BaO and 5.2 wt.% PbO (Table 1).

4.2.8. Sulfides

Sulfide minerals form a volumetrically minor, but environmentally important component of the slag dump (e.g. Lasamis and Norman, 1997). The most abundant and widely dispersed sulfides are pyrrhotite, cubanite, and sphalerite/wurtzite. Both pyrrhotite ($Fe_{1-x}S$) and cubanite ($CuFe_2S_3$) are found intergrown with fayalite crystals, and also occur as round inclusions (< 150 μm in diameter) in interstitial glass (Fig. 4a). Sphalerite/wurtzite [(Fe,Zn)S] generally occurs as acicular needles (up to 80 μm long) or round inclusions (< 50 μm in diameter) scattered throughout the interstitial glass (Fig. 4a). The pyrrhotite contains minor amounts of Bi, Cu, Pb, and Zn (Table 2). Cubanite averages 23 wt.% Cu, and also contains small amounts of Pb (0.36 wt.%) and Zn (3.0 wt.%). The sphalerite/wurtzite in the Penn Mine slags is Fe-rich [average of 22 wt.% Fe (37 mol% FeS)] and contains an average of 1.5 wt.% Cu, 0.11 wt.% Cd, and 42 wt.% Zn. No sulfides are present in the willemite-rich samples.

4.2.9. Metallic Pb and Cu

Small (< 15 μm) inclusions of metallic Pb and Cu occur throughout the slags, and are generally associated with sulfide minerals. EDS spectra indicate that high

Table 2
Electron microprobe analyses of sulfide minerals in Penn Mine slag (wt.%)[a]

Mineral[b]	Fe	Cu	Zn	Cd	Pb	Bi	As	S	Total	n[c]
Pyrrhotite										
Min (Fe)	57.56	0.32	< 0.03	0.05	< 0.05	0.07	< 0.04	40.26	98.87	
Max (Fe)	60.47	0.41	0.17	< 0.04	0.06	< 0.05	< 0.04	40.23	101.43	
Average	62.10	0.27	0.11	< 0.04	0.09	0.08	0.06	40.25	99.24	10
Cubanite										
Min (Zn)	40.49	23.58	0.87	< 0.04	0.81	< 0.05	0.06	33.89	99.70	
Max (Zn)	39.24	19.66	5.38	< 0.04	0.45	< 0.05	0.15	35.60	100.50	
Average	40.21	22.61	2.99	< 0.04	0.36	< 0.05	0.08	35.45	100.60	10
Sphalerite										
Min (Zn)	24.76	2.57	39.15	0.10	< 0.05	0.24	0.05	34.15	101.01	
Max (Zn)	17.41	0.33	48.16	0.11	0.05	0.10	0.10	34.64	100.90	
Average	22.45	1.57	42.18	0.11	0.15	0.20	0.07	33.86	100.58	7

[a] Included in analysis, but not detected: Mn < 0.02, Ni < 0.02, Au < 0.05, Ag < 0.04, Sb < 0.04.
[b] For each phase, full analyses are included for the maximum and minimum concentrations of the metal identified in parentheses.
[c] n, Number of electron microprobe analyses.

Table 3
Average chemical formulas and volume percentages of predominant slag phases

Phase	Formula	Vol.%
(A) Formulas based on electron microprobe compositions		
Fayalite	$Fe_{1.346}Mg_{.410}Mn_{.002}Ca_{.014}Ba_{.002}Cu_{.003}Zn_{.161}Pb_{.001}Al_{.010}Si_{1.023}O_4$	60
Interstitial glass[a]	$K_{.080}Na_{.037}Fe_{.069}Mg_{.044}Ca_{.152}Ba_{.026}Cu_{.105}Zn_{.189}Cd_{.059}Pb_{.462}Al_{.403}Si_{2.116}O_6$	10
Bulk glass[a]	$K_{.073}Na_{.011}Fe_{.988}Mg_{.198}Ca_{.154}Ba_{.028}Cu_{.002}Zn_{.171}Pb_{.001}Al_{.420}Si_{1.883}O_6$	9
Willemite	$Zn_{1.829}Fe_{.023}Mg_{.125}Cu_{.013}Cd_{.002}Al_{.014}Si_{.994}O_4$	5
Zincian spinel	$Zn_{.792}Fe^{II}_{.186}Mg_{.033}Cu_{.026}Fe^{III}_{.793}Ti_{.021}Al_{1.132}Si_{.017}O_4$	4
Magnetite	$Fe^{II}_{.767}Mg_{.074}Ca_{.006}Ba_{.005}Zn_{.222}Fe^{III}_{1.507}Cr_{.004}Ti_{.039}Al_{.341}Si_{.035}O_4$	4
Hyalophane	$K_{.454}Na_{.093}Fe_{.036}Ca_{.025}Ba_{.281}Zn_{.008}Pb_{.077}Al_{1.321}Si_{2.659}O_8$	2
Pyrrhotite	$Fe_{.886}Cu_{.003}Zn_{.001}S$	1
Cubanite	$Cu_{.950}Zn_{.122}Pb_{.005}Fe_{1.923}S_3$	1
Sphalerite	$Zn_{.601}Fe_{.375}Cu_{.023}Cd_{.001}S$	0.5
(B) Stochiometric minerals		
Quartz	SiO_2	2
Pyrite	FeS_2	0.5
Chalcopyrite	$CuFeS_2$	0.5
Galena	PbS	0.5

[a] Formulas of bulk glass and interstitial glass normalized to 6 oxygens.

concentrations of As, Cd, and Sb are also present in these inclusions. Although these "prills" are volumetrically minor phases, they are potentially very reactive and could release significant amounts of trace elements during weathering (Johnson et al., 1982; Lastra and Carson, 1996).

4.3. Chemical and modal abundance in slags

Modal abundances of the predominant slag phases were estimated by point counting using optical microscopy in transmitted and reflected light, in combination with digital mapping of backscattered electron images on the electron microprobe. Based on modal analysis, the Penn Mine slags are characterized by 4 main types, in order of decreasing abundance: *fayalite-rich, glassy, willemite-rich*, and *sulfide-rich* (Table 4). Fayalite-rich and glassy slags predominate south of the tunnel shown on Fig. 1, whereas willemite-rich slags are found only near the smelter foundation (on the surface, and in USGS drill cuttings). Sulfide-rich slags are restricted to the top surfaces of the slag pot casts (Fig. 3). Volume percentages of the main slag phases were determined by estimating the relative amounts of the 4 types of slag (Table 4), and multiplying these values by the average modal mineralogy of each slag type. Table 3 provides

Table 4
Volume percentages and mineralogy of 4 predominant slag types at Penn Mine

Slag type (vol.% of slag deposits)	Phase (vol.%)[a]									
	Fayalite	Bulk glass	Interstitial glass	Willemite	Hyalophane	Zincian spinel	Magnetite	Sulfides	Pyroxene	Metallic Pb and Cu
Fayalite-rich (72)	>50	–	10–50	–	–	–	1–10	1–10	Trace	Trace
Glassy (14)	–	>99	–	–	–	–	–	Trace	Trace	Trace
Willemite-rich (9)	–	–	10–50	>50	1–10	10–50	–	–	–	Trace
Sulfide-rich (5)	10–50	–	10–50	–	–	–	Trace	10–50	Trace	Trace

[a] Trace, <1 vol.%; –, absent.

average chemical formulas and volume percentages for all phases included in the geochemical modeling calculations. These data were used to construct the pie charts in Fig. 5, which show the distribution of Ba, Cd, Cu, Pb, and Zn within various minerals and in two glass phases.

Bulk chemical analyses of 17 samples of slag show the following ranges in major element oxide concentrations (weight percents): Al_2O_3, 1.23–7.75; CaO, 0.29–10.66; FeO_T, 6.64–40.27; MgO, 0.41–4.00; SiO_2, 17.5–51.3; and TiO_2, 0.07–0.30. The total S contents of these samples range from <0.01 to 1.97 wt.%. As shown in Table 5, potentially toxic elements found at elevated concentrations in the slags include As, Ba, Cd, Cu, Pb, Sb, and Zn. These bulk concentrations vary over several orders of magnitude, and are generally highest in the willemite-rich slags.

4.4. Batch extraction tests

Table 6 presents the results of TCLP and SPLP leaching tests on two willemite-rich slag samples (labeled A and B) from Penn Mine. Both samples contain high bulk concentrations of metals and metalloids (Table 6), and were chosen as representative of the most potentially hazardous slag samples. The regulatory limit for Cd in TCLP leachates is exceeded for slag A, and the Pb limit is exceeded for both samples. Dissolved concentrations in the SPLP leachates are much lower than those in the TCLP tests, and all elements are below the TCLP toxicity criteria.

These results are similar to previous studies of slag leaching, which have shown that organic acids (e.g. acetic acid) generally leach higher concentrations of metals than do inorganic acids (e.g. Robbins et al., 1983; Woodley and Walters, 1986; USEPA, 1995; Koren et al., 1996). For a given sample, differences in trace element concentrations between the TCLP and SPLP leachates may be caused by (1) differences in the metal complexing ability of organic vs. inorganic acids, or (2) differences in leachant pH. Research on the dissolution of silicate and oxide minerals by organic acids has shown that monodentate ligands (e.g. acetate ion) have little or no catalytic effect on dissolution rates (Furrer and Stumm, 1986; Bennett and Casey, 1994). Therefore, variations in leachant pH are most likely responsible for differences between the TCLP and SPLP results. Table 6 shows the leachant pH (before sample addition), the initial test pH (immediately following sample addition), and the final leachate pH for each of the TCLP and SPLP tests. The pH of the buffered TCLP leachant

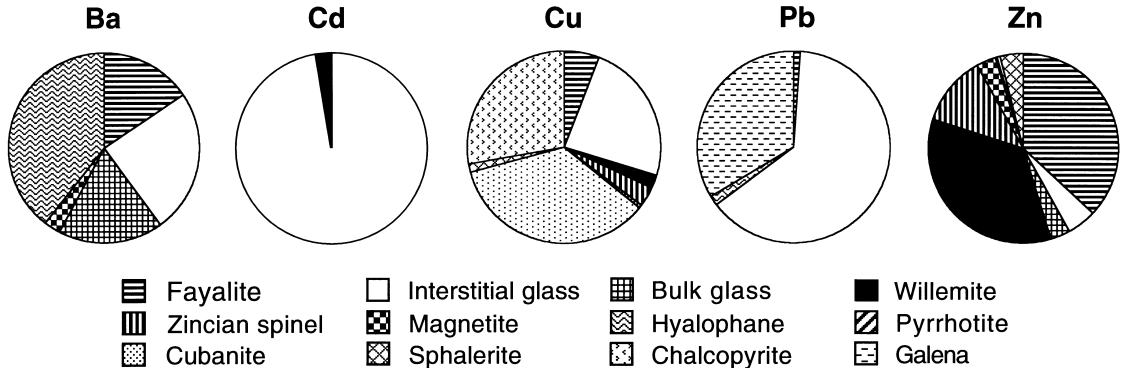

Fig. 5. Pie charts showing the distribution of Ba, Cd, Cu, Pb, and Zn within various minerals and two glass phases in the Penn Mine slag deposits.

Table 5
Selected metal and metalloid concentrations in Penn Mine slags (ppm)[a]

Sample	As	Ba	Cd	Cr	Cu	Fe	Ni	Pb	Sb	Zn	n[b]
Fayalite-rich slag											
Min	15	3200	14	13	1800	15,000	2	161	35	32,000	
Max	320	29,000	110	37	8400	29,000	39	2400	400	77,000	
Average	160	12,000	48	27	5000	22,000	13	1300	230	52,000	10
Glassy slag											
Min	4	1300	32	32	3100	25,000	19	2000	300	52,000	
Max	67	6900	77	46	4400	26,000	42	2400	440	73,000	
Average	37	4400	57	37	3900	26,000	28	2200	370	60,000	3
Willemite-rich slag											
Min	1200	4400	1700	19	22,000	5200	180	22,000	2000	120,000	
Max	5900	13,000	6200	28	40,000	31,000	430	82,000	8200	280,000	
Average	3500	9000	4100	24	30,000	15,000	320	52,000	4100	220,000	3
Sulfide-rich slag											
	9200	5300	14,000	18	64,000	21,000	110	110,000	5,000	140,000	1

[a] Average sample mass: 400 g.
[b] n, Number of ICP–AES or XRF analyses.

Table 6
Trace element concentrations in two samples of willemite-rich slag, and results from TCLP[a] and SPLP[b] extraction tests

Element	TCLP leachate quality criteria[c] (mg/l)	Slag A			Slag B		
		Bulk slag concentration (ppm)	TCLP leachate (mg/l)	SPLP leachate (mg/l)	Bulk slag concentration (ppm)	TCLP leachate (mg/l)	SPLP leachate (mg/l)
As	5.0	5900	0.64	< 0.005	1200	0.056	< 0.005
Ba	100	13,000	0.52	0.25	4400	0.79	0.24
Cd	1.0	6200	2.5	0.20	1700	0.49	0.035
Cr	5.0	19	0.014	< 0.005	24	0.058	< 0.005
Cu	na	40,000	4.1	< 0.005	22,000	50	0.044
Pb	5.0	82,000	30	0.054	22,000	20	0.029
Sb	na	8200	0.008	< 0.003	2000	0.17	< 0.003
Zn	na	280,000	59	1.4	250,000	110	1.1
Leachant pH			4.9	4.9		4.9	4.9
Initial pH (leachant + sample)			4.9	6.2		4.9	6.1
Final leachate pH			4.9	6.5		5.0	6.2

[a] TCLP, toxicity characteristic leaching procedure (USEPA Method 1311).
[b] SPLP, synthetic precipitation leaching procedure (USEPA Method 1312).
[c] TCLP leachate quality criteria used to classify solid wastes as hazardous or non-hazardous (these values are ~100 times the US Interim Primary Drinking Water Standards). No criteria exist for Sb, Cu or Zn, because these elements were not listed in the Primary Drinking Water Standards when the TCLP was developed in 1984 (USEPA, 1996).

remains at approximately 4.9 throughout both TCLP tests, whereas the buffering capacity of the slags causes the SPLP leachant pH to increase throughout both tests, to a final pH value of 6.5 for slag A and 6.2 for slag B. Previous studies have shown that the dissolution rates of most silicate, oxide, and glass phases increase as pH decreases below circumneutral values (e.g. Berner, 1978; Terry, 1983; Knauss et al., 1990).

The TCLP and SPLP extraction tests are conducted under experimental conditions that are very different from the natural weathering environment at Penn Mine. However, the data are useful for comparison with extraction test results on slags from other smelters, and they provide some measure of the relative dissolution kinetics of different slag samples. The results for slags A and B in Table 6 show that the bulk concentrations of trace

elements in the slag are not directly correlated with their leachate concentrations. This demonstrates the importance of understanding slag mineralogy, and the effects of kinetics on slag dissolution.

4.5. Water chemistry

Routine monitoring by EBMUD at sites 1.3 km downstream and 0.8 km upstream of Penn Mine (Golder Associates, 1996), combined with data from this study, provide a general overview of seasonal variations in the Camanche Reservoir water chemistry. Water column profiles indicate that near Penn Mine, the reservoir is relatively well mixed from top to bottom throughout the winter with respect to temperature (18–7.5°C), DO (12–9.9 mg/l), and pH (8.1–7.0). In the late spring and summer, thermal stratification results in three distinct vertical layers: (1) a warm (28–25°C), oxygenated (11–8.9 mg/l), high-pH (8.0–7.1) surface layer (epilimnion), (2) a cooler (18–12°C), O_2-rich (12–10 mg/l), lower-pH (7.2–6.3) bottom layer (hypolimnion), and (3) a zone of highly variable water chemistry between them (thermocline). The cool temperature, high DO, and lower pH of the bottom layer reflect the influence of Mokelumne River water, which enters Camanche Reservoir approximately 1.5 km upstream of Penn Mine and travels along the submerged river channel as a density current (Slotton et al., 1994).

Some water-quality measurements taken at sampling sites near the slag dump revealed chemical conditions very different from those in the adjacent reservoir. Depth profiles taken within the slag depression (site 3, Fig. 1) in August 1996 showed a zone of relatively low pH (6.1) and low DO (0.1 mg/l) in water below 8.0 m depth. This water had a specific conductance of 71 μS/cm, significantly higher than the average conductivity of the lake (32–42 μS/cm). Measurements at the same location during well-mixed conditions in March 1997, January 1998, and March 1998 did not detect this low-pH zone. Groundwater samples collected from USGS well GS-9 (site 5, Fig. 1) in March 1997 contained abundant rust-colored suspended sediment, had a high specific conductivity (500 μS/cm), and a relatively high pH (7.3). According to drill logs in Hamlin and Alpers (1996), this water was sampled from weathered metavolcanic bedrock approximately 0.6 m below the base of the slag dump. In January and March 1998, water within USBM test pit No. 1 (site 4, Fig. 1) was characterized by high pH (8.1–8.3), low DO (1.7–5.9 mg/l), and relatively high specific conductance (79–110 μS/cm).

Table 7 shows selected water-quality data for the slag depression (site 3, Fig. 1), USBM test pit No. 1 (site 4, Fig. 1), USGS well GS-9 (site 5, Fig. 1), and two sites (sites 1 and 2, Fig. 1) in the Camanche Reservoir. These data were collected in March 1997 and March 1998, and represent water compositions during the winter mixis, immediately following or during a drop in reservoir level (see Fig. 2). All measurements are for 0.45-μm filtrates, with the exception of one ultrafiltered sample collected in March 1997 from 0.9 m water depth at site 1. Concentrations of many trace elements in the reservoir waters are higher near the slag dump (sites 2–4) than at the upstream control site (site 1; Table 7, Fig. 6). In particular, filtered (0.45 μm) waters collected from sites 3 and 4 (Fig. 1) contain elevated concentrations of As, Ba, Cd, Cu, Ni, Sb, and Zn, and are taken to represent the chemistry of pore waters in the slag dump. The concentrations of Cd, Cu, and Zn in the slag depression in March 1997 and March 1998 exceed US federal guidelines for the protection of freshwater aquatic life (Table 7; USEPA, 1998). Fig. 6 shows the sum of As, Cd, Cu, Ni, Sb, and Zn concentrations measured in filtered (0.45 μm) waters collected at sites 1–5 (Fig. 1) in March 1997, January 1998, and March 1998. Analyses of waters collected from all 5 sites in August 1996 showed similar spatial trends in trace element distribution, with most concentrations roughly 2 to 3 times higher than the values measured in January 1998 (data for August 1996 are not included in Fig. 6 because of high Zn concentrations in the field blanks). Trace element concentrations are highest at sampling sites located directly within the slag dump (sites 3 and 4, Fig. 1), and reach maximum values when the dump is draining (March 1997, 1998; Fig. 2). The highest metal concentrations were measured in March 1998 during rapid reservoir drawdown following prolonged flooding of the slag deposits (Fig. 6). These data indicate that relatively elevated levels of trace elements are associated with pore waters in the slag dump, and are released to Camanche Reservoir during reservoir drawdown. Metal concentrations in samples collected within 1 m of the downstream edge of the slag dump (site 2, Fig. 1) in March 1997 and 1998 are considerably lower than concentrations at sites 3 and 4 (Table 7). This difference in concentrations probably results from dilution of the slag dump pore waters by mixing with reservoir waters, and transport of metals into the reservoir sediments (Slotton and Reuter, 1995).

As shown in Table 7 and Fig. 6, trace element concentrations in filtered (0.45 μm) water collected from USGS well GS-9 (site 5, Fig. 1) in March 1997 are similar to concentrations at the upstream control site. In this well, most trace elements are associated with the abundant suspended material, as shown by the following unfiltered water analyses (all in μg/l): As, 0.79; Ba, 17; Cd, 4.2; Cu, 15; Ni, 12; and Zn, 17. The unfiltered Fe and filtered SO_4 concentrations (22 and 230 mg/l, respectively) in the well water are significantly higher than the concentrations in Camanche Reservoir; however, they are much lower than the Fe and SO_4 levels in the underlying acidic ground-water plume (Alpers et al., 1999). These data suggest that the water collected from well GS-9 in March 1997 represents a mixture of the Camanche

Table 7
Selected water chemistry and field data for the slag dump depression, USBM test pit No. 1, USGS well GS-9, and 2 sites in the Camanche reservoir

Constituent	Units[a]	Site 1			Site 2		Site 3		Site 4	Site 5		
		Upstream control			Downstream edge of dump[b]		Depression in slag dump		USBM test pit No. 1	USGS well GS-9	Field blanks	
Date	(dd/mm/yy)	17/03/97	17/03/97	16/03/98	17/03/97	16/03/98	18/03/97	16/03/98	16/03/98	18/03/97	17/03/97	16/03/98
Depth	(m)	0.9	0.9	0.9	0.6	0.6	3.0	3.0	0.3	6.1	na	na
Filter pore size	(μm)	0.45	0.005[c]	0.45	0.45	0.45	0.45	0.45	0.45	0.45	0.45	0.45
pH	(Standard units)	6.3	6.3	7.5	7.3	7.6	7.8	7.2	8.3	7.3	na	na
Temperature	(°C)	18	18	9.0	19	16	16	12	13	20	na	na
Specific cond.	(μS/cm)	42	42	50	41	44	41	65	110	500	na	na
Dissolved oxygen	(mg/l)	9.9	9.9	12	13	10	na	7.7	1.7	na	na	na
Alkalinity	(mg/l as $CaCO_3$)	14	14	20	33	18	19	22	28	34	na	na
Ca	(mg/l)	2.0	2.3	5.5	2.9	4.7	4.0	7.3	13	11	< 0.05	< 0.05
Mg	(mg/l)	0.73	0.79	1.3	1.1	1.2	1.2	1.4	1.4	28	0.001	0.006
Na	(mg/l)	1.5	1.5	2.0	1.6	1.8	0.43	2.1	2.4	9.4	< 0.02	< 0.02
K	(mg/l)	0.45	0.47	0.61	0.72	0.67	0.70	0.92	1.2	< 0.01	< 0.01	< 0.01
Cl	(mg/l)	1.2	1.2	2.1	1.3	1.6	< 1.0	1.8	1.8	2.6	na	na
SO_4	(mg/l)	< 1.0	< 1.0	2.7	2.0	2.9	6.2	7.4	20	230	na	na
SiO_2	(mg/l)	3.0	4.1	12	4.7	9.6	3.7	11	7.9	7.4	0.56	2.3
As	(μg/l)	0.27	0.23	0.63	0.38	0.50	0.55	0.72	2.6	0.05	0.07	0.04
Al	(μg/l)	26	4.8	18	33	30	25	21	3.2	1.4	< 0.20	< 0.20
Ba	(μg/l)	14	8.8	13	18	18	94	140	230	6.8	0.65	1.4
Cd	(μg/l)	0.02	< 0.01	< 0.01	0.01	< 0.01	0.61[d]	0.41[d]	0.06	0.19	< 0.01	< 0.01
Cu	(μg/l)	0.65	< 0.10	0.51	0.4	1.5	11[d]	4.6[d]	1.8	< 0.10	< 0.10	< 0.10
Fe	(μg/l)	49	< 3.0	35	41	30	27	41	56	85	< 3.0	< 3.0
Mn	(μg/l)	8.2	4.8	4.9	12	11	15	7.6	25	1.2	0.06	0.06
Ni	(μg/l)	0.22	0.19	0.42	0.38	0.50	0.56	0.55	0.31	1.1	< 0.05	< 0.05
Pb	(μg/l)	1.3	< 0.10	< 0.10	0.15	< 0.10	< 0.10	0.53	< 0.10	< 0.10	0.14	< 0.10
Sb	(μg/l)	0.05	0.03	0.07	0.06	0.10	1.3	2.1	10	0.10	0.09	0.05
Zn	(μg/l)	1.5	0.69	2.1	2.3	6.1	102[d]	250[d]	6.9	1.3	1.6	3.0

[a] μm, Micrometers; mg/l, milligrams per liter; μg/l, micrograms per liter; μS/cm, microsiemens per centimetre; °C, degrees Celsius; na, not analyzed.
[b] Water samples collected within 1 m of downstream edge of slag dump.
[c] Approximate pore diameter of 10,000-Dalton filter membrane.
[d] Water quality criteria to protect freshwater aquatic life (chronic toxicity guidelines, hardness $\leqslant$ 25 mg/l as $CaCO_3$): Cd, 0.38 μg/l; Cu, 3.5 μg/l; Zn, 32 μg/l (USEPA, 1998).

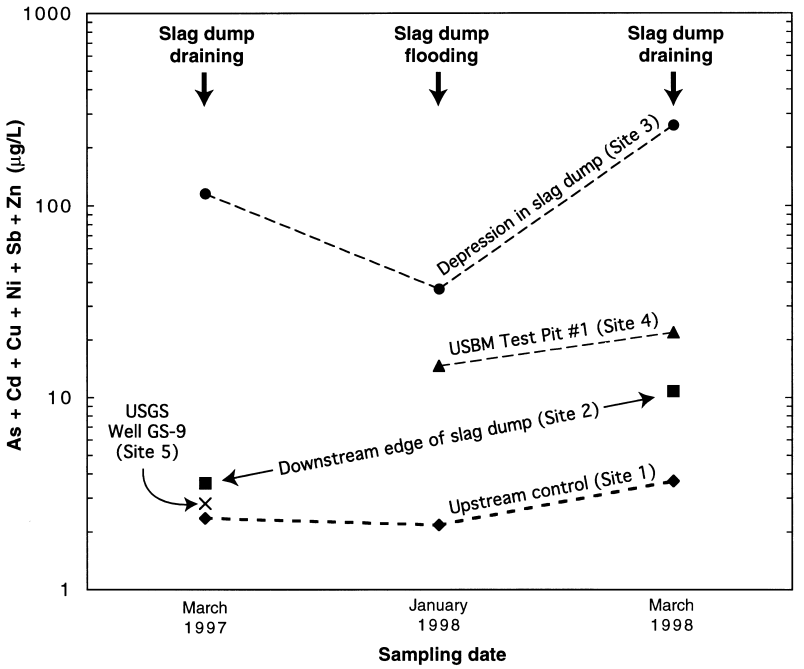

Fig. 6. Sum of As, Cd, Cu, Ni, Sb, and Zn concentrations measured in filtered (0.45 μm) waters collected at sites 1 to 5 (Fig. 1) in March 1997, January 1998, and March 1998.

Reservoir water and relatively uncontaminated ground water near the base of the slag dump.

4.6. Metal fate and transport

Trace element concentrations in unfiltered Camanche Reservoir water, and filtrates from 3 different pore-diameter membranes (0.45, 0.10, and 0.005 μm) reveal the partitioning of metals in the operationally defined dissolved (<0.005 μm), colloidal (0.005–0.45 μm), and suspended (>0.45 μm) phases. Fig. 7 shows the concentrations of Al, Ba, Cd, Cu, Fe, Pb, SiO_2(aq), and Zn in various filtrates collected at site 2 (Fig. 1) in March 1997 and March 1998 (samples for ultrafiltration were collected in March 1997 only). The sharp decrease in Al and Fe concentrations with decreasing filter pore size indicates that these elements are present mainly in particulate material (e.g. clays, hydrous Al- and Fe-oxides). In contrast, the weak correlation between filter pore size and SiO_2(aq) concentrations shows that silica is not a major component in the particulate phases (i.e. diameters >0.005 μm). The high surface area of suspended and colloidal material plays an important role in regulating the dissolved concentrations of many trace elements at near-neutral pH values (Stumm and Morgan, 1996). As shown in Fig. 7, the concentrations of both Cu and Pb (and Cd in the March 1998 data) decrease with decreasing filter pore size, indicating that these metals are associated with (i.e. sorbed, co-precipitated) particulate material. Conversely, the concentrations of Ba, Cd (in the March 1997 data), and Zn do not show a pronounced decrease with decreasing filter pore size, suggesting that these elements are not bound to particulates, but instead are present as free ions or aqueous complexes in the Camanche Reservoir. The slight decrease in Ba, Cd, and Zn concentrations in the ultrafiltered samples may indicate some sorption to colloids with diameters <0.005 μm, or may be an artifact of the ultrafiltration process.

5. Geochemical modeling

Results of field and laboratory investigations reported above were used to develop geochemical models that simulate irreversible (nonequilibrium) mass-transfer reactions between the slag deposits and the Camanche Reservoir. The primary objective of this modeling was to determine the most important geochemical processes controlling the mobilization of metals from the slag dump. Modeling was conducted using Version 8.0 of the EQ3/6 software package, and the supporting "composite" (data0.com.V8.R6) thermodynamic data file (Wolery, 1994). EQ3/6 is composed of two separate computer codes: EQ3NR, a speciation-solubility code, and EQ6, a reaction-path code (Wolery, 1992; Wolery and Daveler, 1992). Both microcrystalline gibbsite and amorphous $Al(OH)_3$ were added to the composite database, along with their respective solubility product constants (log

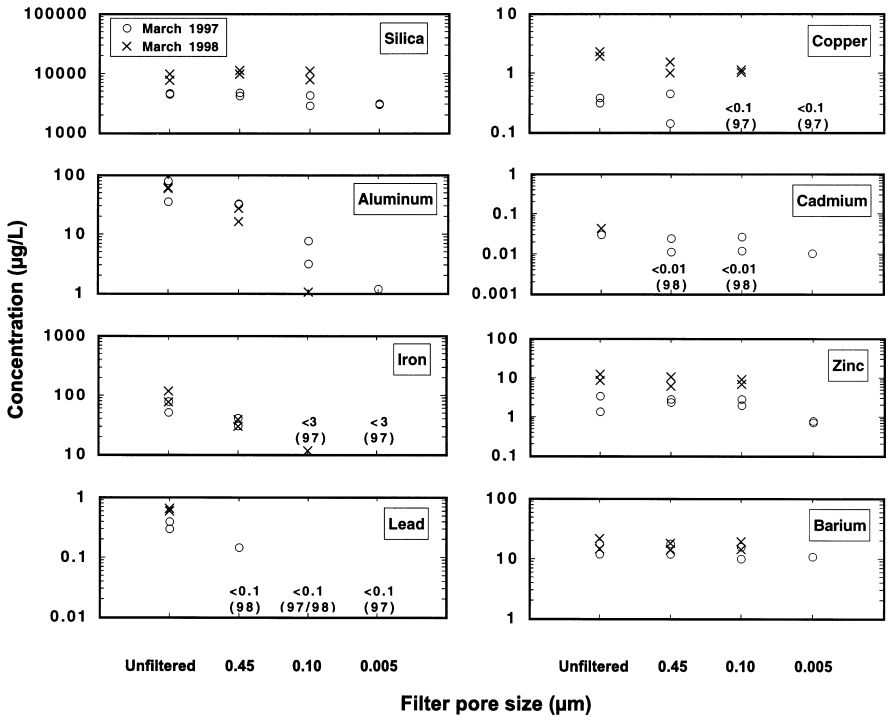

Fig. 7. Concentrations of SiO_2(aq), Al, Fe, Pb, Cu, Cd, Zn, and Ba in unfiltered and filtered (0.45, 0.10, 0.005 μm) Camanche Reservoir water collected near the downstream edge of the slag dump (site 2, Fig. 1) in March 1997 (open circles) and March 1998 (crosses). Analytical detection limits are given in μg/l.

K_{sp} = 9.35, 10.8) and reaction enthalpies (ΔH_r° = −102.508, −110.876 kJ/mol) from Nordstrom et al. (1990). Amorphous $Fe(OH)_3$ was also added, using a log K_{sp} of 4.891 from Ball and Nordstrom (1991). In the model calculations, it is assumed that the reservoir water remains in contact with the atmosphere, as well as any secondary phases that form during the simulations. The length of the reaction period in each model corresponds to the number of days the slag deposits remain fully submerged each year prior to rapid reservoir drawdown (Fig. 2), assuming that this is approximately equal to the residence time of the slag dump pore waters.

5.1. Speciation of initial solution

Irreversible mass transfer between the slag deposits and reservoir waters was simulated by reacting slag of known mineralogy with ultrafiltered water from the upstream control site (Table 7). This water was chosen as an initial solution for the EQ3/6 calculations because it approximates the composition of water flowing into Camanche Reservoir, and because it contains relatively low concentrations of colloids. The fugacities of O_2 and CO_2 were fixed at atmospheric values ($f_{O_2} = 10^{-0.7}$ atm; $f_{CO_2} = 10^{-3.5}$ atm; Stumm and Morgan, 1996), which resulted in DO concentrations similar to those measured in the Camanche surface waters (approximately 10 mg/l). Calculated ionic strengths for the reservoir waters are generally less than 0.005 mol/kg; therefore, the extended Debye-Hückel equation was used to evaluate individual ion activity coefficients (Wolery, 1992). All water analyses were screened for overall charge balance and major inconsistencies before being used for modeling purposes (cf. Ball and Nordstrom, 1991).

The saturation index (*SI*) of an aqueous solution with respect to a mineral is defined by:

$$SI = \log\left(\frac{Q}{K}\right) \quad (1)$$

where Q is the ion activity product and K the equilibrium constant for the dissolution reaction. If the *SI* is zero the water composition reflects solubility equilibrium, a negative value indicates undersaturation, and a positive value indicates supersaturation. Speciation calculations indicate that ultrafiltered lake water is supersaturated with respect to various mineral phases, some of which may be present as colloids (e.g. clays, hydrous Al-, Fe-, and Mn-oxides) with diameters less than 0.005 μm. Both microcrystalline gibbsite and manganite (γ-MnOOH) have saturation indices close to zero (0.89 and 0.56, respectively), indicating that these minerals may exert solubility controls on dissolved Al and Mn concentrations (Alpers and Nordstrom, 1999).

5.2. Porosity and surface area of slag deposits

Field observations and laboratory measurements were used to determine an appropriate mass of slag to react with 1 kg of reservoir water in EQ6. It was assumed that reaction with the finer-grained material between the slag pot casts shown in Fig. 3 controls the composition of pore waters within the slag dump, as this material has the highest total surface area. Petrographic examination of 4 bulk samples (average mass: 2 kg) of these unconsolidated deposits shows that they are composed of 4 main types of slag (Table 4), with minor amounts of lake sediments. This material ranges in size from coarse sand to gravel, with an average porosity of 32% and an average particle density of 4.2 g/cm^3. The porosity (ϕ) of a material is defined as the ratio of the volume of voids (V_V) to the total volume (V_T) ($\phi = V_V/V_T$); therefore, 1000 ml of lake water (i.e. 1 kg) fill the pores of approximately 2100 cm^3 ($V_{SLAG} = V_T - V_V$) of the finer-grained slag deposits (Oelkers, 1996). Multiplying this volume of slag by the average particle density yields a total reactant mass of approximately 8.9 kg.

The total physical surface area of slag in contact with 1 kg of lake water was estimated by sieving the finer-grained material (64 mm to < 0.25 mm) to determine its grain-size distribution. Assuming that the average grain shape is approximated by spheres, the specific geometric surface area (S, cm^2/g) of slag particles in each size fraction is given by (Gregg and Sing, 1982):

$$S = \frac{6}{\rho \cdot d} \tag{2}$$

where ρ is the average particle density (4.2 g/cm^3) and d is the average grain diameter (cm). Multiplying S by the mass of slag retained in each sieve and adding the results yields the total physical surface area for each bulk sample. Dividing this physical surface area by the mass of each sample gives an average specific geometric surface area of 1.5 cm^2/g; therefore, the total physical surface area of 8.9 kg of the finer-grained slag deposits is approximately 13,000 cm^2. This total surface area (1.3 m^2/kg H_2O) lies within the range of physical surface areas compiled by White and Peterson (1990) from studies of silicate aquifer materials with particle sizes and porosities similar to the finer-grained slags (e.g. Gislason and Eugster, 1987). The surface area of each phase in contact with 1 kg of lake water was estimated by multiplying the total physical surface area by the volume percentages shown in Table 3 (assuming that all surfaces are in fluid contact). However, the reactive surface area of each phase (i.e. that surface area which participates directly in chemical reactions) may be very different from the estimated physical surface area because of factors including surface roughness, fluid channeling, and secondary mineral coatings (e.g. White and Peterson, 1990; Brantley and Velbel, 1993; Hochella and Banfield, 1995).

5.3. Rates of slag–water interactions

Table 8 contains kinetic rate expressions for dissolution and oxidation of all slag phases included in the reaction-path calculations. These data were selected based on applicability over the range of pH values in the models, and the ability of EQ6 to reproduce the published experimental data. If kinetic data were not available for the exact composition of a slag mineral, rate parameters were chosen for dissolution of the closest end-member phase. Dissolution and oxidation reactions were assumed to be surface-controlled, and not limited by transport of solutes to and from mineral surfaces (Berner, 1978). Transition state theory (TST) rate laws were used to model the effects of solution composition and distance from equilibrium on dissolution rates. According to TST, minerals dissolve by a mechanism that involves the formation of one or more "activated complexes" (metastable reaction intermediates), which decompose to products in an elementary rate-limiting reaction (Aagaard and Helgeson, 1982). For a more complete discussion of TST, see Eyring (1935), Lasaga (1981), Wieland et al. (1988), Oelkers et al. (1994), and Schott and Oelkers (1995). In EQ6, the TST rate law describing the dissolution rate (r, mol/s) of a mineral in an irreversible reaction takes the form (Delany et al., 1986; Wolery and Daveler, 1992):

$$r = sf\sum_{j=1}^{j_T} k_j \left(\prod_{i=1}^{i_{T,j}} a_i^{-n_{i,j}} \right) \left(1 - e^{-\frac{A}{\sigma_j RT}} \right) \tag{3}$$

Here, s represents the mineral's total physical surface area (cm^2) and f denotes the ratio of reactive to physical surface area (taken as unity in this study). For each reaction mechanism (j), there is a rate constant (k_j, mol/cm^2/s), a kinetic activity product, and a term that depends on the saturation state of the reacting mineral. The kinetic activity product includes the activities of $i_{T,j}$ aqueous species (a_i), each raised to an exponent (n_{ij}) which reflects the stoichiometry of the activated surface complex (Aagaard and Helgeson, 1982). The final bracketed term in Eq. (3) is the affinity factor, where R designates the gas constant, T corresponds to the absolute temperature, σ_j is Temkin's average stoichiometric number (equivalent to the ratio of the rate of destruction of the activated complex relative to the overall dissolution rate, set to one for this study), and A represents the affinity of the overall mineral dissolution reaction (Wolery, 1992):

$$A = -RT\ln\left(\frac{K}{Q}\right) = -2.303RT(SI) \tag{4}$$

Table 8
Rate parameters for dissolution and oxidation of phases in slag

Phase	Rate expressions[a]	E_a[b]	T_{ref}[b]	Reference[c]
Fayalite	$1.1\times10^{-10}[H^+]^{0.69} + 3.2\times10^{-14}$	0	25	(1,2)
Interstitial glass[d]	$5.8\times10^{-10}[H^+]^{0.48}$	84	25	
Bulk glass[e]	$2.7\times10^{-10}[H^+]^{0.63} + 1.8\times10^{-14}$	84	22	
Willemite	$2.3\times10^{-9}[H^+]^{0.45}$	0	22	(2,3)
Zincian spinel[f]	$1.6\times10^{-11}[H^+]^{0.6}$	16	25	(4)
Magnetite	$1.1\times10^{-14}[H^+]^{0.23}$	15	25	(5)
Hyalophane[g]	$1.2\times10^{-10}[H^+]^{0.5}$	36	25	(6)
Pyrrhotite	$2.2\times10^{-12}[O_2(aq)]^{0.5}$	100	22	(7,8)
Cubanite	$1.3\times10^{-11}[Fe(OH)_2^+(aq) + Fe(OH)_3(aq)]^{0.6}$	51	25	(9)
Sphalerite	$1.0\times10^{-11}[Fe(OH)_2^+(aq) + Fe(OH)_3(aq)]^{0.58}$	27	25	(10)
Quartz	1.3×10^{-16}	50	25	(11)
Pyrite	$6.5\times10^{-13}[O_2(aq)]^{0.5}[H^+]^{-0.11}$	88	25	(8)
Chalcopyrite	$1.1\times10^{-12}[Fe(OH)_2^+(aq) + Fe(OH)_3(aq)]^{0.43}$	63	25	(10)
Galena	$3.5\times10^{-8}[Fe(OH)_2^+(aq) + Fe(OH)_3(aq)]^{0.98}$	40	25	(10)

[a] Individual terms in the rate expressions are given as $k_+[X]^{-n}$, where k_+ = forward rate constant (mol/cm^2/s); $[X]$ = activity of aqueous species X; n = exponent of activity term.

[b] All rate constants were adjusted to 15°C in EQ6 using the Arrhenius expression (E_a = activation energy (kJ/mol); T_{ref} = reference temperature for rate constant (°C); Delany et al., 1986). This represents the estimated average temperature of Camanche Reservoir during prolonged flooding of the slag dump in 1997 and 1998 (EBMUD, written comm., 1998).

[c] References: (1) Wogelius and Walther (1992); (2) Westrich et al. (1993); (3) Terry and Monhemius (1983); (4) Terry (1983); (5) White et al. (1994); (6) Schweda (1990); (7) Nicholson and Scharer (1994); (8) Williamson and Rimstidt (1994); (9) Dutrizac et al. (1970); (10) Rimstidt et al. (1994); (11) Brady and Walther (1990).

[d] Dissolution rate constant calculated from TCLP and SPLP test results; E_a and pH-dependency assumed equal to Na–Ca–Al–B–Si glass from Knauss et al. (1990).

[e] Dissolution rate constants and pH-dependency from Parsons et al. (in prep.); E_a assumed equal to Na–Ca–Al–B-Si glass from Knauss et al. (1990).

[f] Dissolution rate assumed equal to $ZnFe_2O_4$ from Terry (1983).

[g] Dissolution rate assumed equal to K-feldspar from Schweda (1990).

where *SI* is the saturation index defined by Eq. (1). At equilibrium ($A = 0$), the affinity factor goes to zero, forcing the reaction rate to do likewise (Oelkers et al., 1994; Schott and Oelkers, 1995).

5.3.1. Silicate and oxide dissolution rates

The dissolution rates of many silicate and oxide minerals are pH-dependent, reflecting the incorporation of H^+, H_2O, or OH^- into rate-controlling surface complexes. The steady-state, far-from-equilibrium dissolution behavior of these minerals produces a U-shaped curve on a log (dissolution rate) vs. pH plot (e.g. Blum and Lasaga, 1988; Brady and Walther, 1989; Oelkers, 1996), with minimum dissolution rates generally observed near the pH_{pzc} (point of zero charge) (Wieland et al., 1988). Far from equilibrium (affinity factor $\cong 1$), the overall dissolution rate is the sum of the rates of the individual reaction mechanisms (Brantley and Chen, 1995):

$$r = sf\left(k_H\left[H^+\right]^{-n_H} + k_W + k_{OH}[OH^-]^{n_{OH}}\right) \quad (5)$$

where k_H, k_W, and k_{OH} represent rate constants for reaction with H^+, H_2O, or OH^-, respectively, and $[H^+]$ and $[OH^-]$ designate concentrations of the indicated aqueous species (assuming unit activities). The exponents n_H and n_{OH} are generally fractional numbers determined by the stoichiometries of H^+ and/or OH^- in the surface complex (Blum and Lasaga, 1988). The rate expressions for silicate and oxide minerals in Table 8 are equivalent to the parenthetical term in Eq. (5). However, most of these expressions consider only the proton-promoted dissolution mechanism, because published data are not available for dissolution at near-neutral and basic pH conditions. Between approximately pH 5 and 8, the dissolution rates of some silicates and oxides become nearly independent of pH (Brady and Walther, 1989); for these minerals, the $k_H\left[H^+\right]^{-n_H}$ term may predict a slightly lower dissolution rate at near-neutral pH than the actual value of k_W. No activity terms are included for quartz, because the dissolution rate is roughly pH-independent between pH 3 and 7.5 (Brady and Walther, 1990). None of the rate expressions in Table 8 include a term for dissolution in high-pH solutions (pH >8), because pH values measured in the Camanche Reservoir are generally less than 8 (Table 7).

5.3.2. Sulfide oxidation rates

Many factors influence the kinetics of sulfide mineral oxidation, including the availability of DO and/or dissolved Fe(III), solution pH, galvanic effects, microbial catalysis, and armoring of mineral surfaces by secondary phases (Perkins et al., 1995; Nordstrom and Alpers, 1999). In the reaction models it is assumed that the lake waters remain in equilibrium with atmospheric O_2; however, O_2 availability may limit reaction rates within the deeper pore waters of the slag dump. Numerous

studies have shown the importance of bacteria (e.g. *Thiobacillus ferrooxidans*) in catalyzing the oxidation of sulfides and dissolved Fe(II) at pH <4 (e.g. Singer and Stumm, 1970). Because the abiotic oxidation of Fe(II) to Fe(III) should be very rapid at the circumneutral pH values measured in Camanche Reservoir (Davidson and Seed, 1983), it is assumed that the effects of microbial catalysis are minimal, and that Fe(II) oxidation is not rate-limiting in the models.

All of the rate expressions for sulfide minerals in Table 8 apply to abiotic oxidation by either DO or Fe(III). An empirical rate law from Williamson and Rimstidt (1994) has been used for the reaction of pyrite with DO that is applicable over 4 orders of magnitude in DO concentration over the pH range 2-10. For pyrrhotite, the reaction rate reported by Nicholson and Scharer (1994) was used for oxidation at atmospheric O_2 concentrations over the pH range 2–6; a similar rate dependency on DO to that of pyrite was assumed. For both pyrite and pyrrhotite, oxidation by Fe(III) may increase these reaction rates and release more H^+ to solution than oxidation by DO alone (Nicholson, 1994). Kinetic data for oxidation of other sulfide minerals are mostly restricted to hydrometallurgical studies using concentrated, strongly oxidizing solutions (Rimstidt et al., 1994; Perkins et al., 1995). To the authors' knowledge, no kinetic experiments have been conducted at circumneutral pH values, and none report reaction rates with respect to DO. For chalcopyrite, galena, and sphalerite, the rates reported by Rimstidt et al. (1994) for reaction with Fe(III) in solutions similar to many acid mine waters (pH $\cong$ 2; $m_{Fe(III)} = 10^{-2}$–10^{-3}) were used. For cubanite, the rate given by Dutrizac et al. (1970) for reaction with Fe(III) in acidic 0.01 M ferric sulfate solutions was used. Both of these studies report reaction rates with respect to the total concentration of Fe(III); however, these molalities must be converted to activities for input into EQ6 [Eq. (3)]. At the pH values measured in the Camanche Reservoir, speciation calculations indicate that greater than 98% of Fe(III) is present as $Fe(OH)_2^+(aq)$ or $Fe(OH)_3(aq)$. Therefore, the activities of these two aqueous species were substituted for $m_{Fe(III)}$ in the TST rate laws (Table 8), assuming that the overall reaction rate with hydrolyzed Fe(III) at near-neutral pH is the same as reaction with the Fe(III) aquo complex ($Fe(H_2O)_6^{3+}$) at low pH (Luther, 1987).

5.3.3. Glass dissolution rates

A dissolution rate for the Pb–Zn–Cu–Cd–Ba-rich interstitial glass phase was estimated using the TCLP and SPLP extraction test results presented in Table 6. Electron microprobe analyses show that interstitial glass hosts > 98 wt.% of the total Cd and Pb in both of these willemite-rich slags. Microprobe data were used to calculate a formula (normalized to 6 oxygens) for the interstitial glass in each slag, and the modal abundance of this phase was estimated by point counting. Representative 500 g samples of both slags were crushed to pass a 9.5-mm sieve (USEPA, 1994, 1996), and surface areas of the unwashed material were measured using a single point N_2 Brunauer–Emmett–Teller (BET) gas adsorption method (Brunauer et al., 1938; Gregg and Sing, 1982). The average specific surface areas of slag A and slag B are 1355 ± 200 cm^2/g and 3388 ± 200 cm^2/g, respectively. For a given extraction test, the total physical surface area of interstitial glass was estimated by multiplying the specific surface area of slag A or B by the total reactant mass (100 g), and the modal percentage of the interstitial glass phase in that slag.

Assuming that all of the Cd and Pb released to solution originated from interstitial glass, dissolution rates (r_g, mol glass/cm^2/s) were calculated using the following expression:

$$r_g = \frac{m_i W_L}{\nu_{i,g} s_g t} \tag{6}$$

where i is the component used to define the dissolution rate (Cd or Pb), m_i refers to the molality of i in the leachate (mol/kg), W_L is the mass of leachant (kg), $\nu_{i,g}$ denotes the number of mol of i in the interstitial glass formula, s_g represents the initial surface area of interstitial glass in each sample (cm^2), and t is the duration of the extraction test (s). Normalized release rates for Cd and Pb are approximately equal for a given test; therefore, the average of both elements was used to calculate the interstitial glass dissolution rate. Averaging the results for both slags, the TCLP dissolution rate is 4.2×10^{-12} mol/cm^2/s, and the SPLP rate is 1.3×10^{-13} mol/cm^2/s. Assuming a similar pH-dependency to the Na–Ca–Al–B–Si glass studied by Knauss et al. (1990), the overall rate constant for dissolution of the interstitial glass is 5.8×10^{-10} mol glass/cm^2/s (Table 8). This relatively high rate constant is consistent with SEM observations of naturally weathered slags, which suggest that interstitial glass reacts more rapidly than fayalite (Fig. 4c). However, these short-term dissolution rates may be considerably higher than long-term, steady-state rates because of (1) initial rapid dissolution of fine-grained particles and reactive surface features generated during crushing, and (2) early incongruent dissolution, with preferential release of network-modifying cations (e.g. Cd, Pb) relative to network formers (e.g. Si, Al) (Brantley and Chen, 1995).

Kinetic data for dissolution of the bulk glass phase were derived from single-pass, flow-through experiments on two samples of glassy slag from Penn Mine (Parsons et al., in prep.). Dissolution rates were measured in buffered solutions (pH 3, 5, 7, and 9), extraction test leachants, and the Camanche Reservoir water at 22°C. Average dissolution rates for the bulk glass phase were calculated from normalized steady-state release rates of

Al, Ba, Cu, Fe, Mg, Pb, Si, and Zn (cf. Knauss et al., 1990). Under acidic conditions (pH 3–6), the dissolution rate constant (k_H) was 2.7×10^{-10} mol glass/cm^2/s, and the order with respect to pH (n_H) was −0.63. At circumneutral pH (pH 7.6–7.8), the dissolution rate constant (k_W) for reaction with Camanche Reservoir water was 1.8×10^{-14} mol glass/cm^2/s (Table 8).

5.4. Modeling results and discussion

Selected results of the EQ6 reaction-path calculations are presented in Table 9, and Figs. 8–10. These models simulate reactions between the slag deposits and the Camanche Reservoir water during submergence of the slag dump from October 1996 to March 1997 (approximately 170 days, see Fig. 2). Table 9 includes predicted final water compositions for 3 separate modeling runs, as well as chemical analyses of unfiltered and filtered (0.10 μm) water collected from the slag depression (site 3, Fig. 1) in March 1997. Assuming that the field data in Table 9 approximate pore-water compositions within the slag dump, predicted concentrations of elements that occur mainly as dissolved species (e.g. Ba, Zn, see Fig. 7) should be comparable to values in the 0.10-μm filtrate. However, because EQ6 does not account for sorption processes (i.e. results are given as total *dissolved* concentrations), predicted concentrations of elements that are predominantly bound to particles >0.10 μm in diameter (e.g. Cu, Pb, see Fig. 7) should be more comparable to total concentrations in unfiltered reservoir water.

Results of preliminary mass-transfer calculations using the field and laboratory data reported above are shown in Table 9 in the column labeled "Run 1." In this simulation, all of the slag phases react with reservoir water at a rate determined by Eq. (3) except for hyalophane, which reaches saturation during the first step of reaction progress and remains supersaturated throughout the reaction period. The model predicts a rapid rise in pH during the first day of reaction (from 6.2 to 7.2), accompanied by a rapid increase in the concentrations of most elements in solution. The fluid quickly reaches supersaturation with respect to a large number of minerals in the EQ3/6 database; however, only those minerals observed as weathering products in the field (e.g. Fig. 4d), or those likely to reach solubility equilibrium at 15°C (Berner, 1978; Nordstrom and Alpers, 1999) were allowed to form. Speciation calculations on all waters collected near the slag deposits were used as a guide to choosing secondary phases that may control dissolved

Table 9
Selected water chemistry from depression in slag dump (March 1997), and results of EQ6 modeling runs

		March 1997 field data from Site 3 (Fig. 1)		EQ6 model results		
				Run 1	Run 2	Run 3
Parameter	Units[a]	Unfiltered	0.10-μm filtrate	Initial run	Calibrated glass dissolution rate[b]	Calibrated sulfide oxidation rate[c]
Temperature	(°C)	16	16	15	15	15
pH	(standard units)	7.8	7.8	8.2	7.9	7.9
Alkalinity	(mg/l as $CaCO_3$)	na	19	43	24	21
Ca	(mg/l)	4.3	3.8	4.7	3.4	3.1
Mg	(mg/l)	1.3	1.2	12	8.0	7.7
Na	(mg/l)	0.84	0.62	1.6	1.6	1.6
K	(mg/l)	0.76	0.69	0.63	0.62	0.62
Cl	(mg/l)	1.3	1.3	1.2	1.2	1.2
SO_4	(mg/l)	6.2	6.2	11	18	10
SiO_2	(mg/l)	4.2	3.9	8.3	4.7	4.7
Al	(μg/l)	52	3.4	0.12	0.11	0.11
Ba	(μg/l)	95	88	98	80	130
Cd	(μg/l)	0.63	0.66	48	0.51	0.48
Cu	(μg/l)	14	9.8	17	16	17
Fe	(μg/l)	67	7.6	4.6	4.6	4.6
Mn	(μg/l)	17	15	0.00032	0.00032	0.00029
Pb	(μg/l)	0.15	<0.10	28	28	3.4
Zn	(μg/l)	108	105	148	127	119

[a] °C, degrees Celsius; mg/l, milligrams per liter; μg/l, micrograms per liter; na, not analysed.
[b] Interstitial glass dissolution rate constant decreased by 1.5 orders of magnitude ($k_H = 2.9\times10^{-11}$ mol/cm^2/s).
[c] All sulfide oxidation rate constants decreased by 2 orders of magnitude.

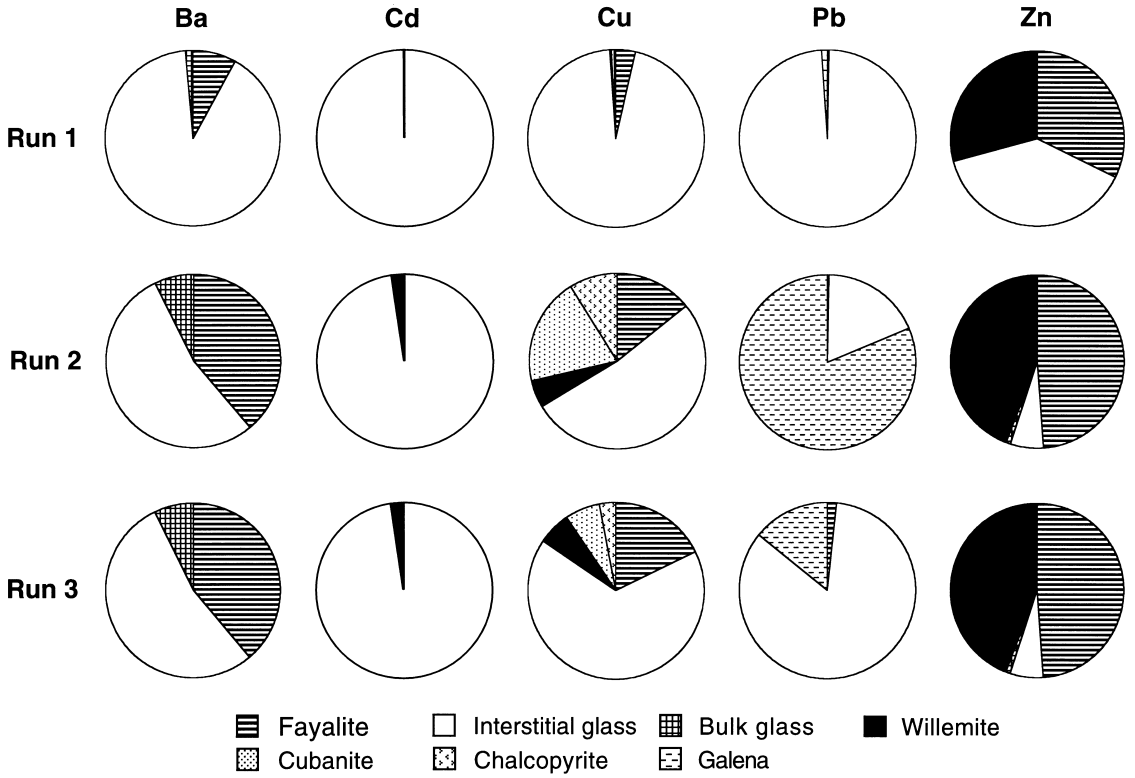

Fig. 8. Pie charts showing the predominant sources of Ba, Cd, Cu, Pb, and Zn released during 3 EQ6 modeling simulations of irreversible mass-transfer between the slag deposits and Camanche Reservoir.

concentrations in the slag dump pore waters. The following phases precipitated during the initial simulation: barite, cerussite, chalcedony (SiO_2), amorphous $Fe(OH)_3$, microcrystalline gibbsite, hydrozincite, manganite, montmorillonite ($Mg_{.495}Al_{1.67}Si_4O_{10}(OH)_2$), and tenorite (CuO). Comparing the final water compositions from Run 1 with the field data in Table 9 shows reasonable agreement for some elements (e.g. Ba, Ca, K, Na); however, the model alkalinity and pH are too high, and the concentrations of many elements (e.g. Cd, Pb, Zn) are overpredicted.

The results of this simulation suggest that the dissolved concentrations of Ba, Cu, Fe, SiO_2, and SO_4 within the slag depression may be controlled by mineral solubilities. Disparity between the predicted and measured values for Al probably results from Al-bearing colloids in the 0.10-μm filtrate (Fig. 7). Inclusion of Mn-bearing colloids could also explain the low predicted Mn value, although solubility control by microcrystalline-to-amorphous Mn-(oxyhydr)oxides is most likely responsible for higher concentrations in the reservoir waters. In the field, the concentrations of most elements are regulated by a combination of processes including adsorption, coprecipitation, formation of metastable phases or solid solutions, and biological activity (Langmuir, 1997).

Additional reaction-path calculations were conducted to test the sensitivity of the model results to uncertainties in the field and laboratory data, and to the various assumptions outlined above. The results of systematic sensitivity analyses demonstrate that the most important variables controlling predicted solution compositions are the (1) dissolution rate of the interstitial glass phase, (2) rates and mechanisms of sulfide oxidation reactions, (3) reactive surface area of the slag deposits, and (4) secondary phases formed during the reaction-path simulation. Changes in surface areas and reaction rates have a similar effect on model results; therefore, it is difficult to distinguish the relative importance of these parameters. Increasing the pH of the initial solution from 6.2 to 7.2 slows the release of most elements from the slag for the first day of reaction, but has little or no effect on the final predicted concentrations after 170 days. Varying the initial mass of slag does not affect model results, because none of the initial reactants are exhausted and a relatively minor amount (0.3–0.8 g) of slag dissolves during each simulation.

Run 2 was designed to resolve the apparent discrepancy between the final predicted concentration of Cd in Run 1 and the values measured at site 3 (Table 9). The pie charts in Fig. 8 show the predominant sources of Ba, Cd, Cu, Pb, and Zn released from the slag

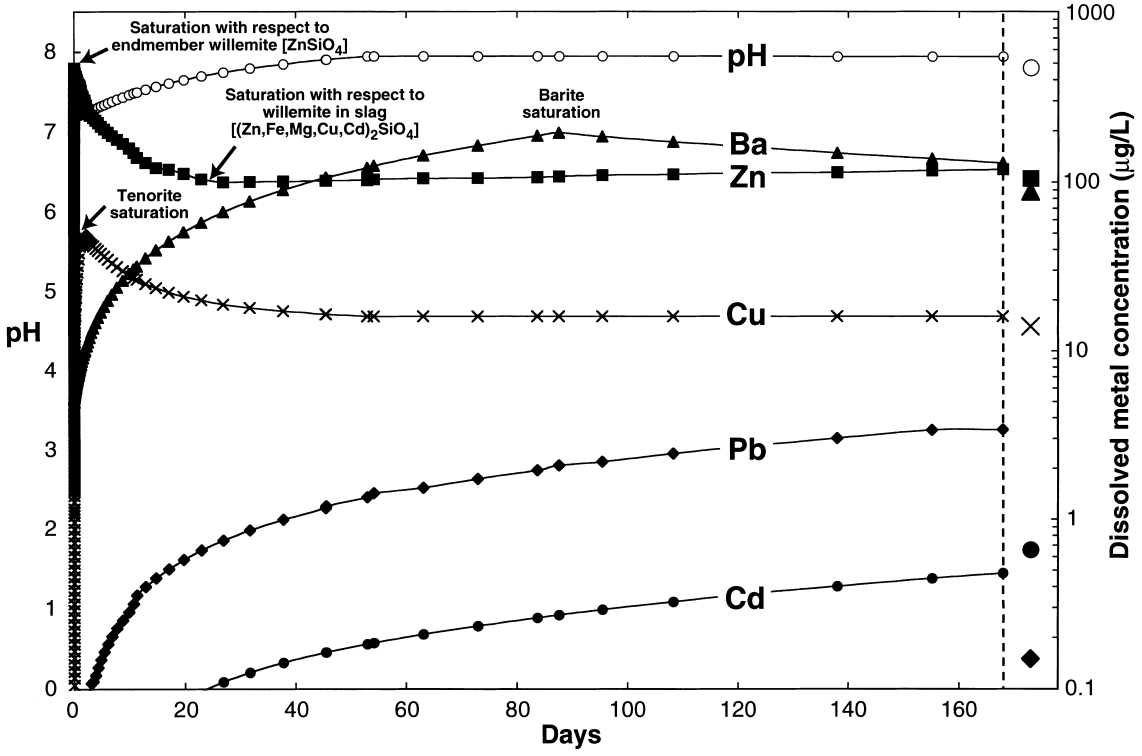

Fig. 9. Dissolved metal concentrations and pH during the Run 3 modeling simulation. Field data from the slag dump depression (Site 3) in March 1997 are represented by larger symbols to the right of the dashed vertical line. Measured concentrations of Cu and Pb are from unfiltered water, whereas Ba, Cd, and Zn concentrations are from a 0.10-μm filtrate.

deposits during the reaction-path calculations. Most of the Cd released to solution in Run 1 originates from the interstitial glass phase (Fig. 8), and the predicted concentration is not limited by the solubility of a secondary mineral. Because the long-term, steady-state dissolution rate of interstitial glass is expected to be lower than the short-term dissolution rate calculated using Eq. (6), the rate constant of this phase was lowered in Run 2 by 1.5 orders of magnitude to obtain a more reasonable predicted value for Cd. As shown in Table 9, this adjustment also lowers the predicted pH, alkalinity, and concentrations of Ca, Mg, and SiO_2 to values closer to those measured in the slag depression. The decrease in pH causes the solution to become undersaturated with respect to hydrozincite; therefore, another Zn-bearing precipitate must be chosen to obtain reasonable predicted Zn concentrations. Hem (1972) suggested that willemite solubility may control Zn levels in natural waters with pH values and SiO_2(aq) concentrations similar to those measured in Camanche Reservoir. Precipitation of willemite in Run 2 results in a final predicted Zn concentration which closely approximates the field data (Table 9); however, kinetic barriers probably limit willemite formation in the natural system. Dissolved Zn concentrations within the slag dump pore waters may be regulated by phases such as hemimorphite ($Zn_4Si_2O_7(OH)_2{\cdot}H_2O$) or amorphous Zn-silicate (Fraval et al., 1997) for which thermodynamic data are not available.

The objective of Run 3 was to resolve differences between the final predicted concentrations of Pb and SO_4 in Run 2 and values measured within the slag depression (Table 9). In Run 2, approximately 80% of the Pb released to solution originates from galena (Fig. 8), whereas SO_4 is derived primarily from oxidation of pyrrhotite (41%), galena (31%), cubanite (13%), and pyrite (9%). In the pore waters of the slag dump, sulfide oxidation is probably limited by the availability of DO and Fe(III), and by the HFO coatings observed on sulfide surfaces (Fig. 4d). Therefore, in Run 3 the oxidation rate constants of all sulfide minerals were lowered by two orders of magnitude to produce final predicted concentrations of Pb and SO_4 closer to those measured in the field (Table 9). The decrease in dissolved SO_4 causes an increase in the final predicted Ba concentration, which is maintained in solubility equilibrium with barite.

Changes in solution pH and dissolved concentrations of Ba, Cd, Cu, Pb, and Zn during the Run 3 simulation are plotted as a function of time in Fig. 9. The cumulative number of mol of product minerals formed

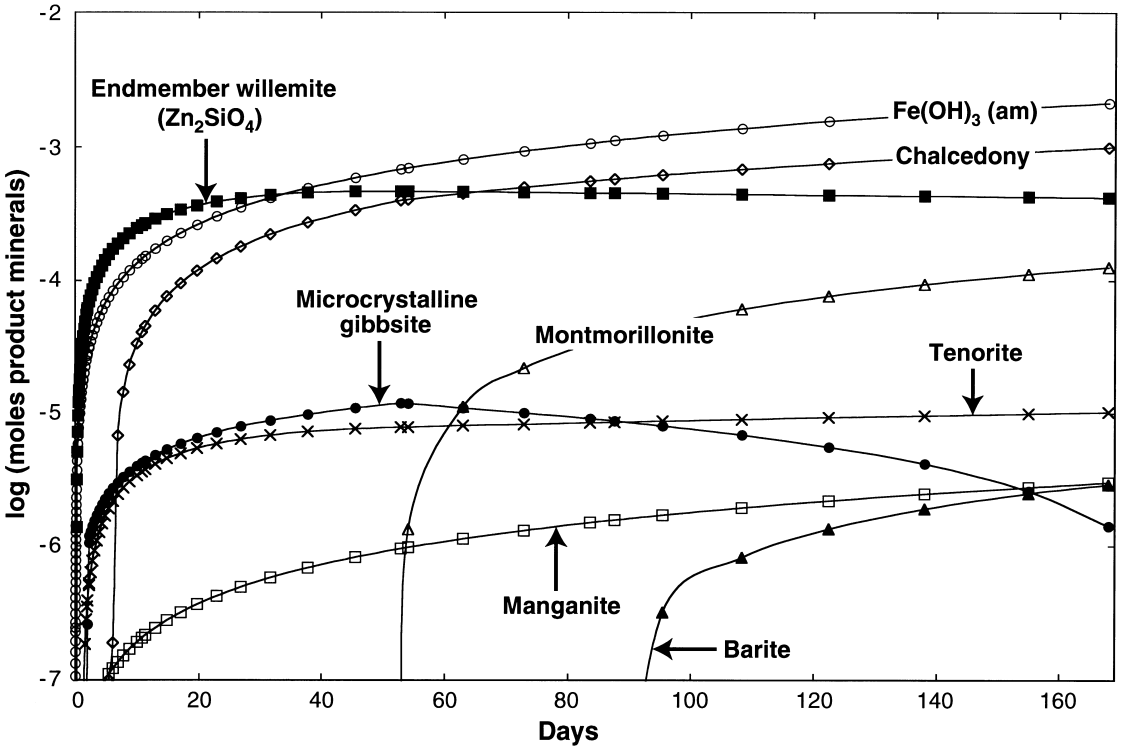

Fig. 10. Secondary minerals produced during the Run 3 modeling simulation of irreversible mass-transfer between Penn Mine slag and Camanche Reservoir water.

throughout the reaction path are shown in Fig. 10. As noted for Run 1, the model predicts a rapid increase in pH during the first day of reaction, accompanied by a rapid rise in the dissolved concentrations of most elements. During the first 6 days of reaction, the following phases precipitate from solution (in order of appearance): microcrystalline gibbsite, manganite, amorphous $Fe(OH)_3$, endmember willemite (Zn_2SiO_4), tenorite, and chalcedony. After 27 days of reaction, the fluid reaches saturation with respect to willemite from the slag deposits (composition given in Table 3), causing the endmember willemite to begin dissolving back into solution. The increasing dissolved Mg concentration results in montmorillonite precipitation after 53 days, which causes the solution to become undersaturated with respect to microcrystalline gibbsite. Barite precipitates after 88 days of reaction; however, the dissolved concentrations of Cd and Pb remain below saturation with respect to any secondary minerals (Fig. 9). Aqueous speciation analyses of all waters collected from the slag depression and USBM test pit No. 1 in March 1997 and March 1998 (Table 7) show barite saturation indices ranging from -0.38 to $+0.53$. This range of SI values may be caused by spatial variations in the mineralogy of the slag deposits, or differences in the residence time of the slag dump pore waters (Fig. 10).

Comparison between the pie charts in Figs. 5 and 8 indicates that some metal-bearing phases in the slag deposits (e.g. hyalophane, zincian spinel) are relatively unreactive in the reservoir waters. In Run 3, dissolution of the interstitial glass phase contributes most of the Ba, Cd, Cu, and Pb to solution, whereas Zn originates mainly from dissolution of fayalite and willemite. Following the calibration of sulfide oxidation rates in Run 3, galena oxidation accounts for 14% of the Pb released to solution, and oxidation of cubanite and chalcopyrite contribute only 6 and 3% of the total Cu release. In the field, the amount of metal released via sulfide oxidation is probably much greater when the slag dump is exposed following reservoir drawdown, and the supply of O_2 is not rate-limiting. These pie charts show the importance of using kinetic rate expressions based on TST when modeling the mobility of trace elements from base-metal slags.

6. Summary and conclusions

The results of this study demonstrate that base-metal slag deposits at the Penn Mine in California are a source of environmental contamination through leaching of potentially toxic elements. Chemical and mineralogical

analyses show that the slag contains relatively high concentrations of As, Ba, Cd, Cu, Pb, and Zn, and that these elements are hosted by a variety of minerals and two glass phases. Examination of leached cavities on naturally weathered slag surfaces indicates that sulfide minerals and a Pb–Zn–Cu–Cd–Ba-rich interstitial glass phase react more rapidly than other slag phases. Measurement of Camanche Reservoir water compositions reveals concentrations of As, Ba, Cd, Cu, Ni, Sb, SO_4, and Zn near the slag deposits that are elevated relative to an upstream control site. These concentrations are highest at sampling sites located directly within the slag dump, and reach maximum values during drawdown. Filter pore-size comparisons indicate that Cu and Pb released from the slag are transported into the reservoir via colloids and suspended sediments, while Ba and Zn are transported mainly as free ions or aqueous complexes. Dissolved metal concentrations decrease with increasing distance from the slag dump as a result of mixing with reservoir waters, and transport of metals into the bottom sediments.

Kinetic modeling of reactions between the slag deposits and the Camanche Reservoir waters suggests that the dissolved concentrations of Al, Ba, Cu, Fe, Mn, SiO_2, and SO_4 in the slag dump pore waters may be controlled by mineral solubilities. Careful selection of secondary phases based on field observations and knowledge of precipitation kinetics (Nordstrom and Alpers, 1999) results in close correlation between predicted and measured concentrations of these elements. Reaction-path calculations show that the main processes controlling metal release from the slag deposits are (1) dissolution of fayalite, willemite, and glass; (2) sulfide oxidation; and (3) secondary phase precipitation. When the slag dump is submerged, sulfide oxidation rates may be limited by the supply of dissolved O_2. Differences between predicted and measured pH values, alkalinities, and dissolved concentrations of Cd and Pb probably result from overprediction of reactive surface areas and/or mineral weathering rates. Lead release may also be affected by other attenuation processes in the natural system, such as sorption or coprecipitation with secondary phases. Sensitivity analyses suggest that field weathering rates are approximately two orders of magnitude lower than published laboratory rates, which is consistent with results from other field studies (e.g. White and Peterson, 1990; Brantley and Velbel, 1993).

The reaction-path models presented in this paper are not unique, but represent an approximation of the major geochemical processes controlling metal release from the Penn Mine slag deposits. Because of the complexity of the natural system and limitations of the EQ3/6 program (Wolery, 1994), the authors have had to make a number of simplifying assumptions in the conceptual models. Nevertheless, it is believed that kinetic modeling of abiotic, irreversible mass-transfer reactions provides important insights into the environmental stability of base-metal slags. When properly constrained through careful field and laboratory studies, this modeling approach can and should be used to develop remediation strategies for slags at both historical and modern smelting sites. In modern base-metal smelters, more efficient smelting technology generally results in slags with lower metal contents than the historical slags at Penn Mine (e.g. Queneau et al., 1991). However, the results of the present study indicate that detailed characterization of slag mineralogy, surface area, dissolution kinetics, and field weathering conditions are still required to predict the long-term (i.e. tens to hundreds of years) reactivity of these metallurgical wastes.

Acknowledgements

The authors would like to acknowledge the enthusiastic support and scientific insights provided by our late friend and colleague Tracy Tingle. Thanks are extended to Roger Ashley, Jennifer Coston, Michael Hunerlach, and James Rytuba of the US Geological Survey for field and laboratory support. We thank Robert Jones for assistance with the electron microprobe, and James Leckie for helpful suggestions throughout this study. Field and laboratory assistance by Kaye Savage, Phil Neuhoff, Thráinn Fridriksson, Kurt Friehauf, and Britt Argow is greatly appreciated. The East Bay Municipal Utility District is gratefully acknowledged for allowing access to their property, and for providing a large-scale base map for field studies. Constructive reviews by Ted Eary, David Koren, David Parkhurst, and Charles Patterson improved our original manuscript. This research was funded through student research grants to MBP from the Geological Society of America, the Northern California Geological Society, and the Stanford School of Earth Sciences Shell and McGee funds. The use of brand names is for identification purposes only, and does not constitute an endorsement by Stanford University or the USGS.

References

Aagaard, P., Helgeson, H.C., 1982. Thermodynamic and kinetic constraints on reaction rates among minerals and aqueous solutions. I. Theoretical considerations. Am. J. Sci. 282, 237–285.

Alpers, C.N., Hamlin, S.N., Hunerlach, M.P., 1999. Hydrogeology and geochemistry of acid mine drainage in ground water in the vicinity of Penn Mine and Camanche Reservoir, Calaveras County, California: Summary report, 1993–1995. US Geological Survey, Water-Resources Investigations Report 96-4287.

Alpers, C.N., Nordstrom, D.K., 1999. Geochemical modeling of water-rock interactions in mining environments. In: Plumlee, G.S., Logsdon, M.J. (Eds.), The Environmental Geochemistry of Mineral Deposits, Part A: Processes, Techniques, and Health Issues. Reviews in Economic Geology, Vol. 6A, Society of Economic Geologists, Littleton, CO, pp. 289–323 (Chapter 14).

Aubury, L.E., 1908. Copper Resources of California. California State Mining Bureau Bull. 50, San Francisco.

Ball J.W., Nordstrom, D.K., 1991. User's Manual for WATEQ4F, with revised thermodynamic data base and test cases for calculating speciation of major, trace, and redox elements in natural waters. US Geological Survey Open-File Report 91–183.

Bäverman, C., Sapiej, A., Moreno, L., Neretnieks, I., 1997. Serial batch tests performed on municipal solid waste incineration bottom ash and electric arc furnace slag, in combination with computer modelling. Waste Manag. Res. 15, 55–71.

Bayless, E.R., Greeman, T.K., Harvey, C.C., 1998. Hydrology and geochemistry of a slag-affected aquifer and chemical characteristics of slag-affected groundwater, northwestern Indiana and northeastern Illinois. US Geological Survey, Water-Resources Investigations Report 91–4198.

Bennett, P.C., Casey, W., 1994. Chemistry and mechanisms of low-temperature dissolution of silicates by organic acids. In: Pittman, E.D., Lewan, M.D. (Eds.), Organic Acids in Geological Processes. Springer-Verlag, Berlin, pp. 162–200 (Chapter 7).

Berner, R.A., 1978. Rate control of mineral dissolution under earth surface conditions. Am. J. Sci. 278, 1235–1252.

Blum, A., Lasaga, A., 1988. Role of surface speciation in the low-temperature dissolution of minerals. Nature 331, 431–433.

Brady, P.V., Walther, J.V., 1989. Controls on silicate dissolution rates in neutral and basic pH solutions at 25°C. Geochim. Cosmochim. Acta 53, 2823–2830.

Brady, P.V., Walther, J.V., 1990. Kinetics of quartz dissolution at low temperatures. Chem. Geol. 82, 253–264.

Brantley, S.L., Chen, Y., 1995. Chemical weathering rates of pyroxenes and amphiboles. In: White, A.F., Brantley, S.L. (Eds.), Chemical Weathering Rates of Silicate Minerals. Reviews in Mineralogy, Vol. 31. Mineralogical Society of America, Washington, DC, pp. 119–172 (Chapter 4).

Brantley, S. L., Velbel, M. A. (Eds.), 1993. Geochemical kinetics of mineral–water reactions in the field and in the laboratory. Chem. Geol. 105, 1-232.

Browne, J.R., 1868. Mineral Resources of the States and Territories West of the Rocky Mountains. Government Printing Office, Washington, DC.

Brunauer, S., Emmett, P.H., Teller, E., 1938. The adsorption of gases in multimolecular layers. J. Am. Chem. Soc. 60, 309–319.

Clark, W.B., Lydon, P.A., 1962. Mines and mineral resources of Calaveras County, California. California Division of Mines and Geology, County Report 2. San Francisco.

Cordone, A.J., 1962. Heavy-metal mining pollution of the Mokelumne River. California Department of Fish and Game, Region II, Inland Fisheries, Rancho Cordova, California.

Davidson, W., Seed, G., 1983. The kinetics of the oxidation of ferrous iron in synthetic and natural waters. Geochim. Cosmochim. Acta 47, 67–79.

Davy Environmental, 1993. Site Characterization Report: Penn Mine, Calaveras County, California. Prepared for California Regional Water Quality Control Board, Central Valley Region.

Delany, J.M., Puigdomenech I., Wolery, T.J., 1986. Precipitation kinetics option for the EQ6 geochemical reaction path code. UCRL-53642, Lawrence Livermore National Laboratory, Livermore, California.

Droop, G.T.R., 1987. A general equation for estimating Fe^{3+} concentrations in ferromagnesian silicates and oxides from microprobe analyses, using stoichiometric criteria. Mineral. Mag. 51, 431–435.

Dutrizac, J.E., MacDonald, R.J.C., Ingraham, T.R., 1970. The kinetics of dissolution of cubanite in aqueous acidic ferric sulfate solutions. Metall. Trans. 1, 3083–3088.

Emery, J.J., 1978. Slags as industrial minerals. In: Coope, B.M. (Ed.), Proceedings of the 3rd "Industrial Minerals" Internat. Congr. Metal Bulletin Ltd., London, pp. 127-142.

Eyring, H., 1935. The activated complex in chemical reactions. J. Chem. Phys. 3, 107–115.

Fällman, A.M., Hartlén, J., 1994. Leaching of slags and ashes — controlling factors in field experiments versus in laboratory tests. In: Goumans, J.J.J., van der Sloot, H.A., Aalbers, Th.G. (Eds.), Environmental Aspects of Construction with Waste Materials. Studies in Environmental Science, Vol. 60. Elsevier, Amsterdam, pp. 39-54.

Ficklin, W.H., Mosier, E.L., 1999. Field methods for sampling and analysis of environmental samples for unstable and selected stable constituents. In: Plumlee, G.S., Logsdon, M.J. (Eds.), The Environmental Geochemistry of Mineral Deposits, Part A: Processes, Techniques, and Health Issues. Reviews in Economic Geology, Vol. 6A, Society of Economic Geologists, Littleton, CO, pp. 249–264 (Chapter 12).

Finlayson, B.J., Rectenwald, H.J., 1978. Toxicity of copper and zinc from the Penn Mine area on king salmon (*Oncorhynchus tshawytscha*) and steelhead trout (*Salmo gairdneri*) in the Mokelumne River Basin, California. California Department of Fish and Game, Environmental Services Branch, Administrative Report 78-1.

Flett, D.S., Riddler, G.P., 1992. Implications of current and future regulations in the EC and North America for the utilisation or disposal of metallurgical slags. In: Minerals, Metals, and the Environment. Institution of Mining and Metallurgy. Elsevier, New York, pp. 43-53.

Fraval, S., Bottero, J.Y., Stone, W.E.E., Broekaert, P., Masin, F., Pirotte, P., Mosnier, F., 1997. NMR evidence of silicate and carbonate competition for cations in solution at low temperature: Case of Ca^{2+}, Zn^{2+}, Pb^{2+}, and Al^{3+}. Langmuir 13, 2550–2556.

Furrer, G., Stumm, W., 1986. The coordination chemistry of weathering: I. Dissolution kinetics of δ-Al_2O_3 and BeO. Geochim. Cosmochim. Acta 50, 1847–1860.

Gee, C., Ramsey, M.H., Maskall, J., Thornton, I., 1997. Mineralogy and weathering processes in historical smelting slags and their effect on the mobilisation of lead. J. Geochem. Explor. 58, 249–257.

Gislason, S.R., Eugster, H.P., 1987. Meteoric water-basalt interactions. II: a field study in N.E. Iceland. Geochim. Cosmochim. Acta 51, 2841–2855.

Golder Associates, 1996. Draft Environmental Impact Report for the Penn Mine Site Long-Term Solution Project. SCH

EIR No. 95103036. Prepared for East Bay Municipal Utility District and Central Valley Regional Water Quality Control Board.

Golder Associates, 1997. Final Environmental Impact Report for the Penn Mine Site Long-Term Solution Project: Comment Response Document. SCH EIR No. 95103036. Prepared for East Bay Municipal Utility District and Central Valley Regional Water Quality Control Board.

Gregg, S.J., Sing, K.S.W., 1982. Adsorption, Surface Area and Porosity, 2nd Edition. Academic Press, London.

Gül, R., 1994. Heavy metal content of the Keban lead plant slag and movement of metals in soil of the surrounding region. Water Poll. Res. J. Canada 29, 531–544.

Hamlin, S.N., Alpers, C.N., 1995. Hydrogeology and geochemistry of acid mine drainage in ground water in the vicinity of Penn Mine and Camanche Reservoir, Calaveras County, California: First-year summary. US Geological Survey, Water-Resources Investigations Report 94-4040.

Hamlin, S.N., Alpers, C.N., 1996. Hydrogeology and geochemistry of acid mine drainage in ground water in the vicinity of Penn Mine and Camanche Reservoir, Calaveras County, California: Second-year summary, 1992-93. US Geological Survey, Water-Resources Investigations Report 96-4257.

Hem, J.D., 1972. Chemistry and occurrence of cadmium and zinc in surface water and groundwater. Water Resour. Res. 8, 661–679.

Heyl, G.R., Cox, M.W., Eric, J.H., 1948. Penn zinc-copper mine, Calaveras County, California. In: Bramel, H.R., Cox, M.W., Eric, J.H., Heyl, G.R., Ransome, A.L., Wyant, D.G. (Eds.), Copper in California. Vol. 144, California Division of Mines Bulletin, pp. 61–84.

Hochella, M.F., Jr., Banfield, J.F., 1995. Chemical weathering of silicates in nature: A microscopic perspective with theoretical considerations. In: White, A.F., Brantley, S.L. (Eds.), Chemical Weathering Rates of Silicate Minerals. Reviews in Mineralogy, Vol. 31. Mineralogical Society of America, Washington, DC, pp. 353–406 (Chapter 8).

Horowitz, A.J., Demas, C.R., Fitzgerald, K.K., Miller, T.L., Rickert, D.A., 1994. US Geological Survey protocol for the collection and processing of surface-water samples for the subsequent determination of inorganic constituents in filtered water. US Geological Survey, Open-File Report 94-539.

Jahanshahi, S., Jorgensen, F.R.A., Moyle, F.J., Zhang, L., 1994. The safe disposal of toxic elements in slags. In: Nilmani, M., Lehner, T., Rankin, W.J. (Eds.), Pyrometallurgy for Complex Materials and Wastes. The Minerals, Metals, and Materials Society, Warrendale, PA, pp. 105–119.

Johnson, E.A., Oden, L.L., Sanker, P.E., 1982. Results of EPA extraction procedure toxicity test applied to copper reverberatory slags. US Bureau of Mines Report of Investigations 8648.

Julihn, C.E., Horton, F.W., 1938. Mines of the Southern Mother Lode Region: Part I — Calaveras County. US Bureau Mines Bull. 413, 112–116.

Knauss, K.G., Bourcier, W.L., McKeegan, K.D., Merzbacher, C.I., Nguyen, S.N., Ryerson, F.J., Smith, D.K., Weed, H.C., Newton, L., 1990. Dissolution kinetics of a simple analogue nuclear waste glass as a function of pH, time, and temperature. Mater. Res. Soc. Symp. Proc. 176, 371–381.

Kontopoulos, A., Komnitsas, K., Xenidis, A., 1996. Environmental characterization of lead smelter slags in Lavrion. In: Minerals, Metals, and the Environment II. Institution of Mining and Metallurgy, London, pp. 405–419.

Koren, D.W., Bédard, P.L., Prud'homme, P.J.A., 1996. Investigations of leach test protocols for slags: Final report. Canada Centre for Mineral and Energy Technology, Mining and Mineral Sciences Laboratories Report 96-10 (CR), Ottawa.

Kucha, H., Martens, A., Ottenburgs, R., De Vos, W., Viaene, W., 1996. Primary minerals of Zn-Pb mining and metallurgical dumps and their environmental behavior at Plombières, Belgium. Environ. Geol. 27, 1–15.

Lagos, G.E., Luraschi, A., 1997. Toxicity characteristic leaching procedure (TCLP) applied to Chilean primary copper slags. Trans. Inst. Min. Metall. (Sect. C) 106, C95–C97.

Lang, H., 1907. The copper belt of California — III. Eng. Mining J. 84, 1006–1010.

Langmuir, D., 1997. Aqueous Environmental Geochemistry. Prentice Hall, New Jersey.

Lasaga, A.C., 1981. Transition state theory. In: Lasaga, A.C., Kirkpatrick, R.J. (Eds.), Kinetics of Geochemical Processes. Reviews in Mineralogy, Vol. 8. Mineralogical Society of America, Washington, DC, (Chapter 4), pp. 135–169.

Lasamis, R., Norman, D.K., 1997. Preliminary study of minerals in Tacoma smelter slags. Washington Geol. 25, 19–25.

Lastra, R., Carson, D., 1996. Mineralogical characterization of deleterious elements in ten slags from Canadian non-ferrous sulfide smelters, Part II. Canada Centre for Mineral and Energy Technology, Mining and Mineral Sciences Laboratories Report 96–35 (CR), Ottawa.

Luther, G.W., 1987. Pyrite oxidation and reduction: molecular orbital theory considerations. Geochim. Cosmochim. Acta 51, 3193–3199.

Male, D.W., Leduc, L.G., Ferroni, G.D., 1997. The potential of mining slag as a substrate for microbial growth and the the microbiological analysis of slag and slag seepage. Antonie van Leeuwenhoek Internat. J. General and Molecular Microbiol. 71, 379–386.

Mandin, D., van der Sloot, H.A., Gervais, C., Barna, R., Mehu, J., 1997. Valorization of lead-zinc primary smelters slags. In: Goumans, J.J.J., Senden, G.J., van der Sloot, H.A. (Eds.), Waste Materials in Construction: Putting Theory into Practice. Studies in Environmental Science, Vol. 71. Elsevier, Amsterdam, pp. 617–630.

Manz, M., Castro, L.J., 1998. The environmental hazard caused by smelter slags from the Sta. María de la Paz mining district in Mexico. Environ. Pollut. 98, 7–13.

Martin, R.C., 1988. Volcanogenic massive sulfide belt of the Western Sierra Nevada Foothills. Califor. Geol. 41, 195–204.

May, A., Peterson, J.B., 1991. Assessment of lead slag landfill site and the use of a computational program for chemical species. In: Lootens, D.J., Greenslade, W.M., Barker, J.M. (Eds.), Proc. Symp. Environmental Management for the 1990s. Society for Mining, Metallurgy, and Exploration, Denver, pp. 217–223.

Millipore Corporation, 1993. Selecting a membrane for concentration, desalting, and buffer exchange of macromolecules (ultrafiltration). Millipore Corp., Bedford, MA, AB002.

Moore, J.N., Luoma, S.N., 1990. Hazardous wastes from large-scale metal extraction. Environ. Sci. Technol. 24, 1278–1285.

Nicholson, R.V., 1994. Iron-sulfide oxidation mechanisms: Laboratory studies. In: Jambor, J.L., Blowes, D.W. (Eds.), The Environmental Geochemistry of Sulfide Mine Wastes.

Mineral. Assoc. Canada Short Course Handbook, Vol. 22. Waterloo, Ontario, pp. 163–183 (Chapter 6).

Nicholson, R.V., Scharer, J.M., 1994. Laboratory studies of pyrrhotite oxidation kinetics. In: Alpers, C.N., Blowes, D.W. (Eds.), Environmental Geochemistry of Sulfide Oxidation. Amer. Chem. Soc. Symp. Ser. 550, Washington, D.C. (Chapter 2), pp. 14–30.

Nordstrom, D.K., Alpers, C.N., 1999. Geochemistry of acid mine waters. In: Plumlee, G.S., Logsdon, M.J. (Eds.), The Environmental Geochemistry of Mineral Deposits, Part A: Processes, Techniques, and Health Issues. Reviews in Economic Geology, Vol. 6A.. Society of Economic Geologists, Littleton CO (Chapter 6), pp. 133–160.

Nordstrom, D.K., Plummer, L.N, Langmuir, D., Busenberg, E., May, H.M., Jones, B.F., Parkhurst, D.L., 1990. Revised chemical equilibrium data for major water-mineral reactions and their limitations. In: Melchior, D.C., Bassett, R.L. (Eds.), Chemical Modeling of Aqueous Systems II. Amer. Chem. Soc. Symp. Ser. 416, Washington, DC (Chapter 31), pp. 398–413.

Oelkers, E.H., Schott, J., Devidal, J.L., 1994. The effect of aluminum, pH, and chemical affinity on the rates of aluminosilicate dissolution reactions. Geochim. Cosmochim. Acta 58, 2011–2024.

Oelkers, E.H., 1996. Physical and chemical properties of rocks and fluids for chemical and mass transport calculations. In: Lichtner, P.C., Steefel, C.I., Oelkers, E.H. (Eds.), Reactive Transport in Porous Media. Reviews in Mineralogy, Vol. 34. Mineralogical Society of America, Washington DC, (Chapter 3), pp. 131–191.

Perkins, E.H., Nesbitt, H.W., Gunter, W.D., St-Arnaud, L.C., Mycroft, J.R., 1995. Critical review of geochemical processes and geochemical models adaptable for prediction of acidic drainage from waste rock. Mine Environment Neutral Drainage Program Project 1.42.1, Canada Centre for Mineral and Energy Technology, Ottawa.

Peterson, J.A., 1985. Geologic map of the Penn Mine, Calaveras County, California. US Geological Survey, Miscellaneous Field Studies Map MF-1797.

Parsons, M.B., Bourcier W.L., Bird, D.K., in prep. Dissolution kinetics of glassy base-metal smelter slags at 22°C: effects of pH and organic acids.

Peterson, J.A., 1988. Distribution of selected trace and major elements around the massive sulfide deposit at the Penn Mine, California. Econ. Geol. 83, 419–427.

Proctor, D.M., Fehling, K.A., Shay, E.C., Wittenborn, J.L., Green, J.J., Avent, C., Bigham, R.D., Connolly, M., Lee, B., Shepker, T.O., Zak, M.A., 2000. Physical and chemical characteristics of blast furnace, basic oxygen furnace, and electric arc furnace steel industry slags. Environ. Sci. Technol. 34, 1576–1582.

Queneau, P.B., May, L.D., Cregar, D.E., 1991. Application of slag technology to recycling of solid wastes. In: Thermal treatment of radioactive, hazardous chemical, mixed and medical wastes. Proc. of the 1991 Incineration Conf., Univ. of California, Irvine, pp. 69–85.

Rimstidt, J.D., Chermak, J.A., Gagen, P.M., 1994. Rates of reaction of galena, sphalerite, chalcopyrite, and arsenopyrite with Fe(III) in acidic solutions. In: Alpers, C.N., Blowes, D.W. (Eds.), Environmental Geochemistry of Sulfide Oxidation. Am. Chem. Soc. Symp. Ser. 550, Washington, DC, (Chapter 1), pp. 2–13.

Robbins, D.A., Bundy, S.D., Stanga, G.R., 1983. Availability of toxic metals from non-ferrous metallurgical slags using various testing procedures. In: Sohn, H.Y., George, D.B., Zunkel, A.D. (Eds.), Advances in Sulfide Smelting. Vol. 2. Metall. Soc. AIME, San Francisco, pp. 923–934.

Schmidt, J.M., 1978. Volcanogenic massive sulfides at Campo Seco (Calaveras County), California. Unpubl. MS thesis, Stanford Univ.

Schott, J., Oelkers, E.H., 1995. Dissolution and crystallization rates of silicate minerals as a function of chemical affinity. Pure Appl. Chem. 67, 903–910.

Schweda, P., 1990. Kinetics and mechanisms of alkali feldspar dissolution at low temperature. Unpubl. PhD thesis, Stockholm Univ.

Shaw, P., Towers, C.L., 1937. Water pollution problems in California. California Fish Game 23, 262–285.

Singer, P.C., Stumm, W., 1970. Acidic mine drainage: the rate-determining step. Science 167, 1121–1123.

Slotton, D.G., Reuter, J.E., 1995. Heavy metals in intact and resuspended sediments of a California reservoir, with emphasis on potential bioavailability of copper and zinc. Mar. Freshwater Res. 46, 257–265.

Slotton, D.G., Reuter, J.E., Goldman, C.R., Jepson, R., Lick, W., 1994. Camanche Reservoir bottom sediment study: Heavy metal distribution and resuspension characteristics. U.C. Davis Institute of Ecology Contribution 40, Davis, California.

Stumm, W., Morgan, J.J., 1996. Aquatic Chemistry — Chemical Equilibria and Rates in Natural Waters, 3rd Edition. Wiley-Interscience, New York.

Tack, F.M.G., Masscheleyn, P.H., Verloo, M.G., 1993. Leaching behavior of granulated non-ferrous metal slags. In: Vernet, J.D. (Ed.), Environmental Contamination. Studies in Environmental Science, Vol. 55. Elsevier, Amsterdam, pp. 103–117.

Terry, B., 1983. Specific chemical rate constants for the acid dissolution of oxides and silicates. Hydrometallurgy 11, 315–344.

Terry, B., Monhemius, A.J., 1983. Acid dissolution of willemite ($(Zn,Mn)_2SiO_4$) and hemimorphite ($Zn_4Si_2O_7(OH)_2H_2O$). Metall. Trans. 14B, 335–346.

US Environmental Protection Agency, 1994. Synthetic precipitation leaching procedure (SPLP): method 1312. In: Test Methods for Evaluating Solid Waste, SW-846, 3rd Edition. (Revision 0, September 1994).

US Environmental Protection Agency, 1995. Applicability of the Toxicity Characteristic Leaching Procedure to Mineral Processing Wastes. Office of Solid Waste, Washington DC.

US Environmental Protection Agency, 1996. Toxicity characteristic leaching procedure (TCLP): method 1311. In: Test Methods for Evaluating Solid Waste, SW-846, 3rd Edition. (Revision III, December 1996).

US Environmental Protection Agency, 1998. Water quality standards. Code of Federal Regulations, Title 40, Part 131, Section 36 (b) (2) (7-1-98 Edition).

van der Sloot, H.A., Heasman, L., Quevauviller, Ph., 1997. Harmonization of Leaching/Extraction Tests. Studies in Environmental Science 70. Elsevier, Amsterdam.

Westrich, H.R., Cygan, R.T., Casey, W.H., Zemitis, C., Arnold, G.W., 1993. The dissolution kinetics of mixed-cation orthosilicate minerals. Am. J. Sci. 293, 869–893.

White, A.F., Peterson, M.L., 1990. Role of reactive-surface-area characterization in geochemical kinetic models. In:

Melchior, D.C., Bassett, R.L. (Eds.), Chemical Modeling of Aqueous Systems II. Amer. Chem. Soc. Symp. Ser. 416, Washington, DC (Chapter 35), pp. 461–475.

White, A.F., Peterson, M.L., Hochella Jr., M.F., 1994. Electrochemistry and dissolution kinetics of magnetite and ilmenite. Geochim. Cosmochim. Acta 58, 1859–1875.

Wiebelt, F.J., Ricker, S., 1948. Penn Mine slag dump and mine water, Calaveras County, California. US Bureau of Mines, Report of Investigations 4224.

Wieland, E., Wehrli, B., Stumm, W., 1988. The coordination chemistry of weathering: III. A generalization on the dissolution rates of minerals. Geochim. Cosmochim. Acta 52, 1969–1981.

Williamson, M.A., Rimstidt, J.D., 1994. The kinetics and electrochemical rate-determining step of aqueous pyrite oxidation. Geochim. Cosmochim. Acta 58, 5443–5454.

Wilson, L.J., 1994. Literature review on slag leaching. Canada Centre for Mineral and Energy Technology, Mineral Sciences Laboratories Division Report 94-3 (CR), Ottawa.

Wogelius, R.A., Walther, J.V., 1992. Olivine dissolution kinetics at near-surface conditions. Chem. Geol. 97, 101–112.

Woodley, N.K.F., Walters, J.V., 1986. Hazardous waste characterization extraction procedures for the analysis of blast-furnace slag from secondary lead smelters. Environ. Progress 5, 12–17.

Wolery, T.J., 1992. EQ3NR, A computer program for geochemical aqueous speciation solubility calculations: Theoretical manual, user's guide, and related documentation (Version 7.0). UCRL-MA-110662-PT-III, Lawrence Livermore National Laboratory, Livermore, California.

Wolery, T.J., 1994. Letter Report: EQ3/6 Version 8: Differences from Version 7. UCRL-ID-129749, Lawrence Livermore National Laboratory, Livermore, California.

Wolery T.J., Daveler, S.A., 1992. EQ6, A computer program for reaction path modeling of aqueous geochemical systems: Theoretical manual, user's guide, and related documentation (Version 7.0). UCRL-MA-110662-PT-IV, Lawrence Livermore National Laboratory, Livermore, California.